Non-equilibrium Models for Diffusive Cavitation of Grain Interfaces

by

Tze-jer Chuang*, Keith I. Kagawa**, James R. Rice, and Leslie B. Sills***

Division of Engineering, Brown University, Providence, RI, 02912, USA

June 1978

Current affiliations:

*Advanced Systems Technology, Westinghouse Electric Corp., Pittsburgh, PA 15221, USA.

**Hawaiian Fluid Power Corp., Honolulu, Hawaii 96819, USA

***As of October 1978, School of Engineering, Tel-Aviv University, Ramat-Aviv, Israel

DISCLAIMER

Abstract

Existing models for the diffusive growth of voids on grain interfaces, at elevated temperature, are for the most part based on quasi-equilibrium assumptions: surface diffusion is assumed to be sufficiently rapid that the cavity has a rounded, equilibrium shape, and hence cavity growth is assumed to be rate-limited only by grain boundary diffusion. However, creep rupture cavities sometimes have narrow, crack like shapes and it is appropriate to investigate non-equilibrium models for diffusive rupture. We do so here by comparing the quasi-equilibrium model to another limiting case based on a narrow, crack-like cavity shape. Criteria for choosing between the models are given on the basis of representative relaxation times for the surface diffusion process, and also by examining the properties of a "self similar" solution for cavity shape. By a suitable choice of parameters which measure the growth rate, this solution can be made to give results corresponding to either limiting case, and aids the interpolation between them. The results suggest that if s is the ratio of the applied stress to that which just equilibrates cavities against sintering, then for circular cavities on a grain boundary with diameter equal to a quarter of their average center-to-center spacing, the quasi-equilibrium mode applies when $s < 1 + 6\Delta$ and the crack-like mode when $s > 2 + 9\Delta$. Here Δ is the ratio of surface to grain boundary diffusivity. Also, the stress dependence of the growth rate and rupture lifetime is established in each case, and the results are discussed in relation to the interpretation of experimental data.

1. Introduction

Under creep conditions, polycrystalline solids often rupture prematurely by the growth and coalescence of grain boundary voids. Experimental findings indicate that a concentrated void population generally forms on grain boundaries oriented in a direction perpendicular to the applied tensile loads [1], [2], [3]. These voids can be nucleated at grain junctions (w-type voids) or at grain boundary inclusion interfaces (r-type voids). Here we investigate the kinetics of void growth by diffusion, giving special attention to non-equilibrium aspects of the problem. Specifically, rather than assuming a quasi-equilibrium void shape (e.g., one of uniform curvatures) during growth, we allow the void shape to be determined as part of the analysis.

Indeed, numerous studies of the growth of voids on a planar grain boundary perpendicular to the applied stress have been made, on the assumption that surface diffusion is rapid enough to give an essentially spherical void shape. Hull and Rimmer [4] and Speight and Harris [5] estimated the time to rupture of a material with an array of spherical voids located on a planar grain boundary in which atoms were transported from the surface of the cavity along the grain interface. A correction to the model was made by Weertman [6], who considered the appropriate boundary condition to be one of zero vacancy flux on the grain boundary at the midpoint between the voids. Vitovec [7] then estimated the strain rate by considering the change in stress acting across the grain boundary which results from changes in the ligament size. Raj and Ashby [8] investigated the combined contributions of nucleation and growth of voids to the rupture lifetime, again assuming a quasi-equilibrium growth model, and have included effects of grain boundary sliding.

However, the assumption of an equilibrium void shape may not always be satisfied, and it is well known that rather elongated rupture cavities are

sometimes observed. Thus Chuang and Rice [9] examined the problem of a long, crack-like cavity located on a planar grain boundary. Their work was limited to a determination of the cavity shape for a given speed of growth. Here we extend that work to a general examination of non-equilibrium cavity shapes, and of relation between applied stress and growth rates over a wide range of conditions. We consider the growth of pre-existing voids along a planar grain boundary, perpendicular to the applied tensile stress and give results for two cases: (i) a long cylindrical void in which case we assume plane diffusive flow in directions perpendicular to the axis of the cylinder, and (ii) an axi-symmetric void, in which case the diffusive flow is also assumed to be axi-symmetric.

We start the analysis with the two limiting cases of slow, quasi-equilibrium growth, in which the void has a rounded shape of uniform curvature (i.e., the case already examined by Hull and Rimmer [4] and others) (Fig. 1a), and of very rapid growth, in which case there is inadequate time for the void to develop a rounded shape and, instead, it remains thin and crack-like (Fig. 1b).

The practical cases lying between these two extremes are difficult to treat mathematically. However, we find that by linearizing the governing equations it is possible to develop a class of self similar solutions, analogous to those of Mullins [10] for grain boundary grooving, in which the cavity radius a varies with time t as $a = c\, t^{1/4}$, where c is a constant. We find that results for large and small c agree, respectively, with the limiting results based on the assumptions of crack-like and quasi-equilibrium void shapes. By interpreting these results and by examining characteristic times for surface relaxation, we are able to provide guidelines as to which of the two simpler limiting cases is most appropriate in given circumstances.

The matter which diffuses from the void surfaces is assumed to flow along the grain boundary, joining the crystals on either side. The crystals themselves

are assumed to move as if they were rigid, rather than elastically deformable, and this is seen to be justified by estimates of representative elastic relaxation times. Indeed, these relaxation times and those associated with various modes of surface shape and grain boundary alteration are given in the appendix.

Preliminary versions of the results given here, as limited to the long cylindrical void model, are given in theses by Chuang [11] and Kagawa [12].

2. Processes in Diffusive Void Growth

In order to understand clearly the processes to be modelled, a description of the mechanisms which govern diffusive void growth and the behavior of the grains and their boundary is presented here.

Indeed, changes in the shape of a void located on a grain boundary can be accomplished by self-diffusion along the surface of the cavity, by bulk diffusion through the lattice, and by evaporation and condensation. It is expected that at temperatures significantly below the melting point of the material it should be more difficult to move an atom (or a vacancy) through the lattice than along a free surface; thus lattice diffusion should be negligible compared to surface diffusion [13]. As the temperature approaches the melting point, however, lattice diffusion should contribute significantly to the total atom flux. In order to more precisely determine which mechanism is dominant, it is useful to compare characteristic relaxation times of a free surface with periodic curvature when atom flux results from lattice diffusion and when it results from surface diffusion (e.g., Mullins [10,14], summarized in the appendix). If τ_s, the characteristic time for surface diffusion, and τ_ℓ, the characteristic time for lattice diffusion, are such that $\tau_s/\tau_\ell < 0.1$, it can be expected that surface fluxes will be the more significant part of matter transport. From typical values of the quantities involved in calculating these characteristic relaxation times for some common metals (see Tables I and II) at temperature $T = 0.5\ T_m$ and $T = 0.8\ T_m$ (T_m is the melting temperature), it is found that surface diffusion, indeed, does dominate over lattice diffusion as the mechanism governing void growth (see Appendix A1 for details). In a similar manner, it is shown in the appendix that the contribution to matter transport by surface diffusion dominates over that by evaporation-condensation (for example $\tau_s/\tau_v < 0.1$, where t_v is

the characteristic time for evaporation-condensation). Thus, at least for this temperature range, surface diffusion will be considered the only mechanism which determines void shape.

Hence, the voids grow by the diffusion of matter along their surfaces toward the void tip. Near the void tip, in the region adjacent to the grain boundary, the atoms may be removed from the void surface either through the void tip and into the grain boundary or through the lattice. An examination of characteristic relaxation times for grain boundary and lattice diffusion reveals that grain boundary diffusion will be the dominant mechanism (see Appendix A2 for details). As atoms diffuse into the grain boundary, there are various ways for the grains to respond to this additional matter. On the one hand, if grain boundary diffusion is sufficiently fast (with respect to void growth) so that the diffused atoms spread over the entire grain boundary, then the growth of the grain boundary δ will be uniform or equivalently the grains on both sides of the boundary will separate evenly (Fig. 2a). Hence the grains behave as though they are rigid. If, on the other hand, diffusion is slow on the boundary, the grains must deform in order to accommodate the atoms which have accumulated near the void tip. In order to do this the grains deform elastically in this region (Fig. 2b). A first analysis of the accommodation of diffused matter by elastic deformation of the grains has been given by Chuang [11], who examined a semi-infinite crack-like void along an infinite grain boundary. (Chuang's techniques have been adopted in a recent paper by Vitek [15]. However, the conditions assumed along the void surface in [15] involve a discontinuity in the void profile, in that a portion of the void is presumed to have a constant thickness; this discontinuity is inconsistent with the equations governing surface diffusion and it is not clear as to what effect this has on the end results.) Indeed, a comparison of the elastic relaxation time with a time calculated on the basis of the rigid grain assump-

tion (i.e. no elastic effects) indicates that the elastic effects generally occur on a time scale so short as to be negligible (see Appendix A3).

3. Governing Equations

It is known from diffusion theory that differences in chemical potential constitute a thermodynamic force causing atoms to migrate from regions of high potential to those of low potential. In cases of small departures from equilibrium, the general assumption is that the rate of kinetic change along the diffusion path is everywhere linearly dependent on the gradient of the chemical potential.

Thus for diffusion along a free surface, treated as isotropic in the plane of the surface for simplicity, the flux law has the form

$$J_s = - (D_s \delta_s / \Omega kT) \, \partial \mu / \partial s \quad . \tag{1}$$

Here J_s is the number of atoms per unit time crossing unit length in the surface, $\partial/\partial s$ is a derivative with respect to arc length along the surface in the flow direction, μ is the chemical potential per atom, Ω the volume per atom, kT the energy-per-atom measure of temperature, D_s the surface diffusivity, and δ_s the thickness of the diffusion layer. Experimentally, D_s and δ_s cannot be separated and we adopt the expression $\delta_s = \Omega^{1/3}$.

When a thin layer of matter is added to a curved surface, the surface area and hence the total surface energy is altered and thus there is an extra energy change in addition to that of adding matter to the bulk. Herring [16,17] has analyzed the problem and, since the increase in area is negatively proportional to the curvature where matter is added, we have

$$\mu = \mu_o - \gamma_s \Omega (\kappa_1 + \kappa_2) \tag{2}$$

where κ_1, κ_2 are the principal curvatures (positive for voids like those in Fig. 1), γ_s the surface free energy, and μ_o is the potential of the bulk. Here it is assumed that there is no normal stress and the strain energy associated with stresses in the plane of the surface is neglected. Stresses are

very small even at the void tip for the diffusive processes considered and the neglect of the strain energy term is readily justified (e.g., [11]).

Furthermore, conservation of matter requires that for the axisymmetric void,

$$(\Omega/r)\ \partial(rJ_s)/\partial s = v_n \tag{3}$$

where v_n is the normal velocity, or recession rate, of the void surface relative to the adjoining solid material, and where r is the radius measured perpendicularly from the axis of symmetry. For the cylindrical void (i.e., the case of plane diffusive flow) we merely delete the two r's. Hence the differential equation relating position and time dependent changes of the void profile is

$$(B/r)\partial[r\partial(\kappa_1 + \kappa_2)/\partial s]/\partial s = v_n \tag{4}$$

for the axisymmetric void, with

$$B = D_s\delta_s\Omega\gamma_s/kT \quad , \tag{5}$$

and for the cylindrical void the same equation applies with the r's deleted and κ_2 set to zero. The parameter B has dimensions of $(\text{length})^4/(\text{time})$, and has a fundamental role in the subsequent development.

Similarly, for diffusion along the planar grain boundary, also treated as isotropic in its plane, the atom flux rate is

$$J_b = -(D_b\delta_b/\Omega kT)\partial\mu/\partial r \quad . \tag{6}$$

where D_b is the grain boundary diffusivity and δ_b the "thickness" of the diffusion zone. Now we observe that where a thin layer of matter is added at a flat segment of grain boundary, joining the crystals on either side, there is no change in area of the interface and hence no contribution of grain boundary free energy γ_b to μ. However, to insert the matter it is necessary to do

negative work against the normal stress σ acting on the grain boundary at the place of insertion, so that the chemical potential is

$$\mu = \mu_o - \Omega\sigma \quad . \tag{7}$$

Again, the strain energy term is neglected, justly so [11].

For conservation of mass it is necessary that

$$(\Omega/r)\partial(rJ_b)/\partial r + \partial\delta/\partial t = 0 \tag{8}$$

for the axisymmetric geometry, where we define δ as the effective thickening at the grain boundary due to adding matter to the adjoining grains. For the cylindrical void geometry, with plane flow, we replace ∂r by ∂x (the x axis lies in the grain boundary, Fig. 1) and delete the two r's. Hence, in view of the above expressions for J_b and μ, the stress distribution and thickening in the grain boundary are related by

$$(D_b\delta_b\Omega/kTr)\partial[r\partial\sigma/\partial r]/\partial r + \partial\delta/\partial t = 0 \tag{9}$$

for the axisymmetric void. Again $\partial r \to \partial x$ and the two r's are deleted in the cylindrical case.

Since we regard the grains as rigid, $\partial\delta/\partial t$ is uniform as depicted in Figure 2a. The more elaborate models explored by Chuang [11] and Vitek [15] regard the grains as elastically deformable so that δ is itself coupled to the stress distribution σ.

Now, eqs. (4) and (9) are the differential equations to be solved, respectively, on the free surface (to determine its shape) and on the grain boundary (to determine its stress distribution). The regions in which the equations apply are themselves time dependent because the void grows along the grain boundary, and the solutions are coupled by continuity conditions at the void tip where it joins the grain boundary. First we note that the tip itself must

have the equilibrium angle, from balance of local surface thermodynamic forces (as discussed, for example, in the analysis of grain boundary grooving [10]), so that

$$2\gamma_s \cos \psi = \gamma_b \tag{10}$$

where ψ is defined (see Fig. 1) so that $\pi - \psi$ is the angle between the grain boundary and the tangent to the void surface at the tip. Furthermore, the chemical potential must be continuous at the void tip (otherwise there would be an unbounded flux J there) and given the previous expressions for μ this implies that

$$\sigma_o = \gamma_s(\kappa_1 + \kappa_2)_{tip} \tag{11}$$

where σ_o is the normal tensile stress at the void tip and the curvatures are evaluated at the void tip. Recall that $\kappa_2 = 0$ for the cylindrical void. Finally, continuity of flux at the void tip implies that

$$(J_b)_{tip} = 2(J_s)_{tip} \quad ; \tag{12a}$$

whence

$$\sigma_o' = (2kT/D_b\delta_b)\,(J_s)_{tip}$$

$$= (2D_s\delta_s\gamma_s/D_b\delta_b)[\partial(\kappa_1 + \kappa_2)/\partial s]_{tip} \tag{12b}$$

where σ_o' is the first derivative of the normal stress with respect to r or x (whichever is applicable) at the void tip.

The mathematical problem of determining the rate of void growth, for a given average tensile stress acting on the grain boundary, is too difficult to solve in generality. Nevertheless, it is useful to consider the "ideal" solution procedure. We should let the cavity radius a vary with time in an arbitrary, yet to be determined manner, and determine the void shape by solving (4) subject to the conditions that the void height is zero and its slope angle

is ψ at the void extremities, $r = a(t)$. Hence the void shape is a <u>functional</u> of the unknown function $a(t)$, and therefore σ_o and σ_o' of eqs. (11) and (12b) are, in principle, determined as functionals of $a(t)$. We next solve (9) for the stress distribution σ on the grain boundary, subject to given values σ_o and σ_o' at $r = a(t)$ and, for example, to a condition that the flux vanish midway between voids on the grain boundary. These three conditions over-determine the second order differential equation (9) for σ, and hence the value of $\partial\delta/\partial t$ (uniform along the grain boundary for the rigid grains model) that is compatible with given values of σ_o and σ_o' is determined also. But since these latter two quantities are functionals of $a(t)$, the stress distribution $\sigma(r, t)$ on the grain interface, and hence the average stress, is likewise determined, in principle, as a functional of $a(t)$. But the average stress is to be regarded as a <u>prescribed</u> function of time, and its relation to $a(t)$ therefore provides a nonlinear hereditary relation from which the <u>actual</u> history $a(t)$ of void growth is to be determined.

As remarked, this program of solution is too difficult to carry out in general. We therefore limit consideration to histories $a(t)$ which are very slow (quasi-equilibrium, spherical void shape) or very fast (thin, crack-like void shape), and try to judge the intermediate cases on the basis of characteristic relaxation time estimates (appendix) and the solution for one tractable family of growth histories, namely, self-similar growth with $a(t) \propto t^{1/4}$.

4. Void Shapes

Our goal is to determine the boundary conditions σ_o, σ'_o at the void tip in relation to the time history of void growth. This is done here first for the limiting cases of slow, quasi-equilibrium growth and rapid, crack-like growth, and then for a family of intermediate cases based on self-similar solutions. The question arises, for a given history $a(t)$ of cavity growth, how can we determine if we are close to one or another of the limiting cases? This can be done by first computing relaxation times associated with the attainment of equilibrium by surface diffusion, for initial disturbances from equilibrium with half-wavelengths that we identify with the void diameter $2a$. Thus for the long cylindrical void, we set $\ell/2 = 2a$, $L = \infty$ in eq. (A-11) to obtain a characteristic relaxation time

$$(\tau_s)_{\text{cylinder}} = (16/\pi^4)\, a^4/B \simeq a^4/6B\,, \tag{13}$$

B is defined in eq.(5). For the axisymmetric geometry we should set $\ell/2 = L/2 = 2a$, since the void curves in two directions, and this gives a lower relaxation time

$$(\tau_s)_{\text{axisym}} = (4/\pi^4)\, a^4/B \simeq a^4/24B\,. \tag{14}$$

Next we observe that a/v, where $v \equiv da/dt$ is the cavity growth speed, is a characteristic time associated with altering the equilibrium shape towards which the cavity surface is ever-proceeding by surface diffusion. Thus if $\tau_s \ll a/v$, or if

$$a^3 v/B \ll 6(\text{cylinder}) \quad \text{or} \quad 24(\text{axisym.})\,, \tag{15}$$

the cavity shape will be at equilibrium, whereas if $\tau_s \gg a/v$, or if

$$a^3 v/B \gg 6(\text{cylinder}) \quad \text{or} \quad 24(\text{axisym.})\,, \tag{16}$$

the cavity shape will remain effectively unrelaxed and growth will occur

in a crack-like mode. It may be observed that in the early stages of creep rupture a^3 and, presumably, v are small, but both increase in time. Hence it is possible that the early stages of growth occur in a quasi-equilibrium mode and the latter stages in a crack-like mode.

4.1 Quasi-equilibrium Void Shapes

As previously discussed, when a^3v is sufficiently small the void retains a quasi-equilibrium shape of uniform curvature during growth. Thus the cylindrical void is composed of two circular cylindrical segments or caps and the axisymmetric void of two spherical caps.

4.1.1 Long Cylindrical Void (Circular cylindrical caps)

For this case $\kappa_2 = 0$ and (see fig. 1a)

$$\kappa_1 = \sin\psi/a \ . \tag{17}$$

Moreover, as a result of continuity of matter flux at both void tips

$$d[2a^2 f(\psi)]/dt = 2[2\Omega(J_s)_{tip}] \tag{18}$$

where the quantity in brackets on the left is the void volume per unit length along the cylindrical axis and where

$$f(\psi) = (\psi - \sin\psi \cos\psi)/\sin^2\psi. \tag{19}$$

Note that in this case one cannot directly evaluate the flux into the tip by using the last form of (12b); this is because, effectively, the curvature gradient is very small and D_s very large for near-equilibrium growth. Hence from eqs.(11) and (12b) we obtain

$$\sigma_o = \gamma_s \sin\psi/a \ , \quad \sigma_o' = (2kT/\Omega D_b \delta_b) f(\psi) av \tag{20}$$

for the associated stress boundary conditions at the void tip.

4.1.2 Axisymmetric Void (Spherical Caps)

For this case the analogous expressions are

$$\kappa_1 = \kappa_2 = \sin\psi/a \tag{21}$$

and

$$d[(4\pi/3)a^3\, h(\psi)]/dt = 2\pi a[2\Omega(J_s)_{tip}] \ , \tag{22}$$

where the bracketed term on the left is void volume and

$$h(\psi) = [1/(1 + \cos\psi) - (\cos\psi)/2]/\sin\psi \ . \tag{23}$$

Thus the boundary conditions on stress are

$$\sigma_o = 2\gamma_s \sin\psi/a \ , \quad \sigma_o' = (2kT/\Omega D_b \delta_b)\, h(\psi) a v \ . \tag{24}$$

This method of evaluation of σ_o and σ_o' coincides with that by Hull and Rimmer [10] and in related studies.

4.2 Crack-Like Shape

In this limit we assume that $a^3 v$ is sufficiently large and that there is inadequate time for the large amounts of diffusive mass transfer necessary to establish a rounded, near-equilibrium void shape. Instead, the void remains thin and crack like with relatively small curvatures everywhere except near its tip (Fig. 1b) where κ_1 and its gradient must be large in order to allow sufficient mass flow for the characteristic tip angle ψ to develop. Assuming that the speed v does not change appreciably over distances comparable to the void thickness near the tip, the near tip shape is determined by the "steady state" analysis of Chuang and Rice [9]. In that analysis the

void shape near the tip was assumed to remain unchanged, relative to an observer moving with the tip, during growth. This is an appropriate assumption for the high speed limit of void growth, as will be shown mathematically in the next section. The curvature and surface flux rate at the tip are then given by (see Eqs. (24) and (20) of [9]).

$$\kappa_{tip} = 2 \sin(\psi/2) \, (v/B)^{1/3} \tag{25}$$

$$(J_s)_{tip} = 2 \sin(\psi/2) \, (B/\Omega) \, (v/B)^{2/3} \tag{26}$$

where B is defined by (5) and it is noted that $2\sin(\psi/2) = (2\gamma_b - \gamma_s)^{1/2}/\gamma_s^{1/2}$. (To make contact with the notation of [9], we note first that the sign convention for κ is reversed here, and also that in [9] a term ν representing the surface density of diffusing atoms is employed, and this term is replaced here by $\nu = \delta_s/\Omega$. Further, the above expressions actually represent the first term in a certain series solution, but were shown in [9] to be accurate to approximately 2% when compared to the exact, numerically obtained solution for steady state growth.) The corresponding expression for the thickness, 2ω, of the void in steady-state growth, at distances back from the tip on the order of a few times the tip radius of curvature, is [9]

$$2\omega = 4 \sin(\psi/2) \, (B/v)^{1/3} \, . \tag{27}$$

By substituting κ_{tip} and $(J_s)_{tip}$ into (11) and (12b), we find that the values of the stress and its gradient at the tip for consistency with the presumed crack-like mode of growth are

$$\sigma_o = 2\gamma_s \sin(\psi/2) \, (v/B)^{1/3} \tag{28}$$

$$\sigma_o' = 4\gamma_s \sin(\psi/2) \, (D_s\delta_s/D_b\delta_b) \, (v/B)^{2/3} \, . \tag{29}$$

While these results were derived for plane diffusive flow, we note that they are valid not only for rapid growth of the long cylindrical void but also for general 3-D voids, including the axisymmetric void. This is because at rapid growth speeds the principal curvature κ_1 is large near the tip in the direction of growth whereas the curvature κ_2 remains small. For example, $\kappa_2 = \sin\psi/a$ at the tip of the axisymmetric cavity whereas κ_1 is the inverse of the near-tip radius of curvature, and is much larger for growth in a narrow, crack-like mode. Thus, in the rapid growth limit, the state of flow near the axisymmetric void tip approaches a plane flow state (see the next subsection) and (28), (29) are valid for that case also.

4.3 Linearization of Equations for Void Shape

As stated previously, it is desirable to have general solutions for cases of void growth that correspond with neither of the two limiting cases just discussed. Such solutions have not been found for general void growth, but to make the governing equations more tractable the assumption is made that the slope of the void is everywhere small with respect to unity. That is, we linearize the governing equations. For most metals this assumption ($\psi << 1$) is violated at the void tip; see Table III. It can be shown, however, that the results from the linearized analysis for the void tip curvature and flux rate, and hence for σ_o and σ_o', do not differ significantly from the exact solutions in the previous two subsections for a large range of ψ values.

To accomplish the linearization we let $w = w(x,t)$ or $w(r,t)$ be the height of the void surface above the x or r axis in Fig. 1, we set $\partial/\partial s = \partial/\partial x$ or $\partial/\partial r$, and write $\kappa_1 = \partial^2 w/\partial x^2$ for the cylindrical void, or $\kappa_1 = \partial^2 w/\partial r^2$ and $\kappa_2 = (1/r)\partial w/\partial r$ for the axisymmetric void. Further, the

recession rate $v_n = \partial w/\partial t$. Thus Eq.(4) governing the surface shape reduces to

$$B\nabla^2\nabla^2 w + \partial w/\partial t = 0 \tag{30}$$

with

$$\nabla^2 = \partial^2/\partial x^2 \quad \text{or} \quad \nabla^2 = \partial^2/\partial r^2 + (1/r)\partial/\partial r \tag{31}$$

for the two cases, respectively.

For boundary conditions at x or $r = a(t)$, one must have

$$w[a(t),t] = 0, \quad w'[a(t),t] = -\psi \tag{32}$$

where the prime denotes differentiation with respect to x or r. Furthermore, conditions of symmetry at the void center must be met. For the cylindrical void these have the form $w'(0,t) = w'''(0,t) = 0$; the latter condition implies zero matter flux at $x = 0$, and is to be replaced by the condition $(\partial/\partial r)\,[\nabla^2 w(0,t)] = 0$ for the axisymmetric void.

To obtain quasi-equilibrium solutions for the linearized problem, we merely neglect the $\partial w/\partial t$ term. Then for both cases one obtains

$$w = (\psi/2)\,(a - r^2/a) \tag{33}$$

(replace r with x for the cylindrical void), which is the linear approximation to a circular cylindrical or spherical cap. Further, one may compare the void tip curvature $\kappa_1 = \psi/a$ predicted from the linearized analysis with (17) or (21) and, evidently, it differs from the exact quasi-equilibrium result only insofar as ψ differs from $\sin\psi$.

To examine the case of rapid growth within the linearized theory, it is convenient to make the substitution

$$R = (a-r)/(B/v)^{1/3} \tag{34}$$

and to write

$$w(r,t) = (B/v)^{1/3}\, \hat{w}(R,t) \tag{35}$$

in the equations governing axisymmetric void growth. Note that $(B/v)^{1/3}$ is a characteristic length associated with surface diffusion near a disturbance that moves with speed v ; see, for example, Eq.(27). Hence R and $\hat{w}$ are coordinates of the void profile as scaled by this length. Further, let

$$\varepsilon = (B/a^3 v)^{1/3} \tag{36}$$

be the ratio of this characteristic length to the void radius; we are interested in the limit $\varepsilon \to 0^+$. In terms of $\hat{w}$, the differential equation for axisymmetric void growth is readily shown to take the form

$$\frac{\partial^4 \hat{w}}{\partial R^4} + 2\varepsilon \frac{a}{R} \frac{\partial^3 \hat{w}}{\partial R^3} - \varepsilon^2 \frac{a^2}{r^2} \frac{\partial^2 \hat{w}}{\partial R^2} + \varepsilon^3 \frac{a^3}{r^3} \frac{\partial \hat{w}}{\partial R}$$

$$+ \frac{\partial \hat{w}}{\partial R} + \varepsilon \frac{a\dot{v}}{3v^2} R \frac{\partial \hat{w}}{\partial R} + \varepsilon \frac{a}{v} \frac{\partial \hat{w}}{\partial t} = 0 \tag{37}$$

Now, proceeding in the spirit of boundary layer theory, we focus on the limit of the above equation as $\varepsilon \to 0^+$ with R remaining finite. One can view this limit as being one of extremely slow surface diffusivity, $B \to 0^+$. There results

$$\partial^4 \hat{w}/\partial R^4 + \partial \hat{w}/\partial R = 0 \ .$$

It is straightforward to show that the same equation results, as $\varepsilon \to 0^+$, when a similar analysis is done for the long cylindrical void case. Further the equation has the unique solution, bounded for large R,

$$\hat{w} = (\partial w/\partial R)_{R=0} [1 - \exp(-R)] = \psi[1 - \exp(-R)] \tag{38}$$

or

$$w = (B/v)^{1/3} \psi \{1 - \exp[-(a-r)/(B/v)^{1/3}]\} \tag{39}$$

for r near a. This result of the analysis is, of course, just the linearized version of the crack-like void profile discussed earlier and, indeed, this solution for w leads to a curvature and flux rate at the tip which differ from the exact results of Eqs.(25) and (26) for the crack-like limit only insofar as ψ differs from $2 \sin(\psi/2)$. We do not present the details here, but the same boundary layer technique can be applied to the full nonlinear equation (4) describing the void profile. The results confirm that the solution as $\varepsilon \to 0^+$ is the same for the axisymmetric and cylindrical geometry, and coincides with the "steady state" solution of Chuang and Rice [9] outlined earlier.

4.4 Self-Similar Solution for Void Shape

Eq.(30) is seen by dimensional considerations to have a family of "self-similar" solutions that correspond to an increase in void radius with time according to

$$a = \xi_o (Bt)^{1/4} \tag{40}$$

where ξ_o is an arbitrary positive constant. The associated void profile is

such that

$$w = (Bt)^{1/4} \psi \; \eta(\xi) \quad \text{where} \quad \xi = (x \text{ or } r)/(Bt)^{1/4} , \tag{41}$$

and where the function $\eta(\xi)$ must satisfy

$$d^4\eta/d\xi^4 - (\xi/4)\, d\eta/d\xi + \eta/4 = 0 \tag{42}$$

for the long cylindrical void, or

$$d^4\eta/d\xi^4 + (2/\xi)\, d^3\eta/d\xi^3 - (1/\xi^2)\, d^2\eta/d\xi^2$$

$$+ (1/\xi^3 - \xi/4)\, d\eta/d\xi + \eta/4 = 0 \tag{43}$$

for the axisymmetric void. Evidently, $\xi = \xi_o$ corresponds to the void tip, and the conditions

$$\eta(\xi_o) = 0 , \qquad \eta'(\xi_o) = -1 \tag{44}$$

must be met there. Further, it may be anticipated that small values of ξ_o correspond to near-equilibrium conditions and large values to crack-like conditions. Solutions can be found in a power series form

$$\eta = \sum_{m=0}^{\infty} A_m \xi^m \tag{45}$$

and results are discussed in the following subsections.

4.4.1 Long Cylindrical Void

Of the four linearly independent solutions to Eq.(42) for η, two can be discarded for failure to meet the symmetry conditions $\eta'(0) = \eta'''(0) = 0$. There remains

$$\eta = A_o[1 + \sum_{m=1}^{\infty} g_o(m)\xi^{4m}] + A_2\xi^2\,[1 + \sum_{m=1}^{\infty} g_2(m)\xi^{4m}] , \tag{46}$$

$$g_o(m) = \frac{-1}{(4)^{2m}(m!)\ (4m-1)[(4m-2)\ (4m-6)\cdots(2)][(4m-3)\ (4m-7)\cdots(1)]} \tag{47a}$$

$$g_2(m) = \frac{1}{(4)^{2m}(m!)\ (4m+1)[(4m+2)\ (4m-2)\cdots(6)][(4m-1)\ (4m-5)\cdots(3)]} \tag{47b}$$

and where the constants A_o and A_2 are determined in terms of ξ_o by imposing the conditions (44).

4.4.2 Axisymmetric Void

In this case the differential equation (43) for η has a regular singular point at $\xi = 0$ where, in view of the symmetry conditions, one has

$$\eta'(0) = 0\ , \quad [\eta'''(\xi) + \eta''(\xi)/\xi - \eta'(\xi)/\xi^2] \to 0 \quad \text{as} \quad \xi \to 0. \tag{48}$$

The general solution for η consists of four linearly independent solutions, two of which have logarithmic terms that become unbounded at $\xi = 0$. The above boundary conditions are met if the coefficients of these logarithmic solutions are set to zero, and there remain the terms

$$\eta = B_o\left[1 + \sum_{m=1}^{\infty} f_o(m)\xi^{4m}\right] + B_2\xi^2\left[1 + \sum_{m=1}^{\infty} f_2(m)\xi^{4m}\right] \tag{49}$$

where

$$f_o(m) = \frac{(-1)(3)\cdots(4m-5)}{(4)^{4m}(m!)^2\ [1\cdot3\cdots(2m-1)]^2} \tag{50a}$$

and

$$f_2(m) = \frac{(1)(5)\cdots(4m-3)}{(4)^{4m}(m!)^2\ [3\cdot5\cdots(2m+1)]^2} \tag{50b}$$

and B_o and B_2 are determined from the boundary conditions (44) as quotients of series in ξ_o .

Expressions for curvature and flux at the void tip will not be shown in detail because of the complexity of the series expressions. These expressions can easily be derived, however, from

$$(\kappa_1)_{tip} = -(\psi/a)\ \xi_o \eta''(\xi_o)\ ,\quad (\kappa_2)_{tip} = \psi/a \tag{51}$$

$$(J_s)_{tip} = (B\psi/\Omega a^2)\ [-\xi_o^2\ \eta'''(\xi_o) - \xi_o \eta''(\xi_o) - 1] \tag{52}$$

Further, the corresponding value of the stress and its gradient at the void tip are, from (11) and (12b)

$$\sigma_o = (\psi\gamma_s/a)\ [-\xi_o \eta''(\xi_o) + 1] \tag{53}$$

$$\sigma_o' = 2(D_s\delta_s/D_b\delta_b)\ (\psi\gamma_s/a^2)\ [-\xi_o^2\ \eta'''(\xi_o) - \xi_o \eta''(\xi_o) - 1] \tag{54}$$

Note that the series representation for any of these quantities is amenable to numerical computation. In addition, the velocity can be derived by differentiating equation (40) to obtain

$$\xi_o^4 = 4(a^3 v/B)\ . \tag{55}$$

Note that $a^3 v/B$ is the same dimensionless speed measure which occurred in our earlier discussion based on relaxation times.

4.5 Discussion

Indeed, in order to develop a model of void growth using the various solutions found for the various stages of void growth, it would be instructive to compare the similarity solution to the equilibrium, as well as the

crack-like solutions. For very small choices of ξ_o (corresponding to slow void growth) a good approximation to η from both (46) and (49) can be made by neglecting all but the first terms of the series; in this case

$$\eta = (\xi_o/2)\,[1 - (\xi/\xi_o)^2] \tag{56}$$

which is identical to equation (33) for the linearized equilibrium solution. Thus, the self-similar void shape approaches that of the linearized equilibrium void shape when $a^3 v/B$ is chosen to be very small. Furthermore, the shapes predicted by the similarity solution for $\xi_o = 1,2$ and 3 are compared to the linearized equilibrium shape in Fig. 3. Note the good agreement for the void shape in the neighborhood of the void tip; indeed, this is the region of interest since continuity of flux and chemical potential are enforced here in solving the complete void rupture problem.

On the other hand, for larger choices of ξ_o (i.e. for higher growth rates) the similarity solution for the **axisymmetric void is compared to the** crack-like solution in Fig. 4a and Fig. 4b. The shapes are not alike since by fixing ξ_o an acceleration and higher order time derivatives, as well as a velocity are imposed at the void tip. In fact, examination of the acceleration reveals a deceleration at the void tip. Hence, the combination of both this deceleration and the high velocity associated with large choices of ξ_o allows matter to be removed from the void tip to form a depression. But once again the agreement in the neighborhood of the void tip for these two solutions is quite good.

Furthermore, since we are most interested in determining the values of the curvature and flux at the void tip, it is worthwhile to make a comparison

of these quantities as obtained from the various "linearized" solutions.

Figure 5a is a graph of non-dimensionalized curvature at the void tip vs. the void growth rate parameter a^3v/B. It is seen that for slow growth the curvature found from the similarity solution and that derived by the linearized equilibrium solution agree well. For larger values of the growth rate parameter the curvature obtained from the similarity solution and that obtained from the linearized crack-like solution are in close agreement.

Next consider Fig. 5b which is a graph of non-dimensionalized flux at the void tip vs. the void growth rate parameter. Again as in the case of the curvature κ_1, for slower growth rates the equilibrium solution and the similarity solution for the flux at the void tip are in good agreement; furthermore, for $a^3v/B > 4$ the similarity solution acts as a smooth transition into the crack-like solution. Thus it can be concluded that near the void tip and for $a^3v/B < 4$, either the equilibrium solution or the similarity solution approximates well the void growth behavior; for faster growth rates (i.e., $a^3v/B > 100$) the crack-like solution can be used to describe this phenomenon. Moreover, the results are consistent with our earlier discussion of the relaxation time of surface self-diffusion for the axisymmetric void, in which we have suggested $a^3v/B \approx 24$ as representative in separating the two limiting cases.

5. Rigid Grain Model and Stress vs. Growth Speed Relations

As discussed in Section 2, the grains can be assumed to separate rigidly as atoms diffuse into the grain boundary ahead of the void tip. Recall that elastic effects in the grains may be neglected under most circumstances since the elastic relaxation time is much shorter than any representative time of the void growth process. In this section, using the rigid grain assumption the relationship between void growth and applied stress will be explored for each of the void shapes considered in Section 4 (i.e. equilibrium, self similar, and crack-like) and in both two and three dimensions.

5.1 Long Cylindrical Void

In order to model the growth of voids on a grain boundary transverse to an applied stress, consider a very large crystal with a periodic array of symmetric, cylindrical voids of length $2a$ and center to center spacing $2b$ located on a planar grain boundary as shown in Fig. 6a. A uniform stress σ_∞ is applied perpendicular to the grain boundary and at a distance large compared to $2b$.

The differential equation governing the normal stress $\sigma(x)$ at the grain boundary is given by equation (9) and is to be solved subject to the rigid grain assumption that the boundary thickening rate is independent of x. The boundary conditions are that the stress σ_o and its gradient σ_o' are specified at $x = a$, and that the flux J_b, and hence the derivative $\partial\sigma/\partial x$, vanishes at $x = b$.

These conditions require that

$$\partial\delta/\partial t = (D_b\delta_b\Omega/kT)\sigma_o'/(b-a) \tag{57}$$

and that the stress distribution be given by

$$\sigma = \sigma_o + \sigma_o'(x-a)[1-(x-a)/2(b-a)] \ . \tag{58}$$

We regard the average remotely applied stress, σ_∞, as being specified and this is given by

$$\sigma_\infty = \frac{1}{b}\int_a^b \sigma\, dx = (1 - d)\,\sigma_o + (1 - d)^2\, b\sigma_o'/3 \tag{59}$$

where $d \equiv a/b$.

Recalling now that σ_o and σ_o' are expressed, in general, as functionals of the growth function $a(t)$, the last equation relates the unknown growth to σ_∞, regarded as given. As remarked, it is presently possible to carry out the analysis only for special cases. Thus, for quasi-equilibrium growth σ_o and σ_o' are given by eqs. (20), resulting in

$$\sigma_\infty = \frac{1-d}{d}\frac{\gamma_s \sin\psi}{b} + \frac{2}{3}\, d(1 - d)^2\, \frac{kTb^2}{\Omega D_b \delta_b}\, f(\psi)\, v \tag{60}$$

where $f(\psi)$ is defined by (19) and reduces to $2\psi/3$ in the linearized approximation. Note that the speed v appears only in the last term and, if we solve for v,

$$v = \frac{3\Omega D_b \delta_b}{2d(1-d)^2 kTb^2 f(\psi)}\left[\sigma_\infty - \frac{1-d}{d}\frac{\gamma_s \sin\psi}{b}\right] \tag{61}$$

we find the anticipated cut-off stress level below which sintering occurs.

At the other extreme of void growth in the limiting crack-like case, σ_o and σ_o' are found from eqs. (28) and (29), and the expression for σ_∞ is

$$\sigma_\infty = \frac{2\gamma_s \sin(\psi/2)(1-d)}{b}\left[\left(\frac{b^3 v}{B}\right)^{1/3} + \frac{2}{3}\,\Delta(1-d)\left(\frac{b^3 v}{B}\right)^{2/3}\right] \tag{62}$$

where we have introduced the notation

$$\Delta \equiv D_s \delta_s / D_b \delta_b \quad . \tag{63}$$

In this case the speed is related to σ_∞ by

$$v = (27/64)(B/b^3\Delta^3)[(1 + \Sigma\Delta)^{1/2} - 1]^3/(1-d)^3 \tag{64}$$

where

$$\Sigma \equiv 4\sigma_\infty\, b/[3\gamma_s \sin(\psi/2)] \quad . \tag{65}$$

5.2 Axisymmetric Void

Next consider an array of axisymmetric voids of radius a with average center to center spacing $2b$ located on a planar grain boundary as shown in Fig. 6b. As in the case of long cylindrical voids a uniform stress σ_∞ is applied transverse to and far from the grain boundary. The stress distribution is to be determined by solution of equation (9) subject to the given values σ_o and σ_o' at $r = a$ and to zero flux, $\partial\sigma/\partial r = 0$, at $r = b$. Hence there results

$$\partial\delta/\partial t = 2(D_b\delta_b\Omega/kT)\sigma_o' a/(b^2 - a^2) \tag{66}$$

and the stress distribution is

$$\sigma = \sigma_o + [a\sigma_o'/(1 - a^2/b^2)][\ell n(r/a) - (r^2 - a^2)/2b^2] \ . \tag{67}$$

The normal stress in the grain boundary can now be related to the applied stress σ_∞ through

$$\sigma_\infty = \frac{1}{\pi b^2}\int_a^b 2\pi r\sigma\, dr = (1 - d^2)\sigma_o + (1 - d^2)^2\, Qb\sigma_o'/3 \tag{68}$$

where, again, $d = a/b$ and the function $Q = Q(d)$ is defined by

$$Q \equiv [3d/(1 - d^2)^3][\ell n(1/d) - (3 - d^2)(1 - d^2)/4] \ . \tag{69}$$

This function is evaluated in Table IV. We note that Q is not strongly variable over an appreciable range of d values; for example, it lies between approximately 0.5 and 0.65 for all values of $d > 0.1$ (i.e., for voidage in excess of 1% of the grain boundary area).

For quasi-equilibrium void growth σ_o and σ_o' are given by (24) so that

$$\sigma_\infty = 2\,\frac{1-d^2}{d}\,\frac{\gamma_s \sin\psi}{b} + \frac{2}{3}\,d(1 - d^2)^2\, Q\,\frac{kTb^2}{\Omega D_b\delta_b}\,h(\psi)v \tag{70}$$

where $h(\psi)$ is defined by (23) and reduces to $3\psi/8$ upon linearization. Thus the growth rate is given by

$$v = \frac{3\Omega D_b \delta_b}{2d(1-d^2)^2 QkTb^2 h(\psi)} \left[\sigma_\infty - 2 \frac{1-d^2}{d} \frac{\gamma_s \sin \psi}{b} \right] \tag{71}$$

under these conditions.

On the other hand, for growth at the crack-like limit σ_o and σ_o' are given by eqs. (28) and (29) so that

$$\sigma_\infty = \frac{2\gamma_s \sin(\psi/2)(1-d^2)}{b} \left[\left(\frac{b^3 v}{B} \right)^{1/3} + \frac{2}{3} \Delta(1 - d^2) Q \left(\frac{b^3 v}{B} \right)^{2/3} \right] . \tag{72}$$

This can be solved for v to give

$$v = (27/64)(B/b^3\Delta^3)[(1 + Q\Sigma\Delta)^{1/2} - 1]^3/Q^3(1 - d^2)^3 \tag{73}$$

where Σ has been defined in (65) and Δ in (63).

5.3 Comparisons Based on the Similarity Solution

The similarity solution provides, at the price of linearization, a means of interpolating approximately between the quasi-equilibrium and crack-like limiting cases. Our discussion here is limited to the axisymmetric model; a Sc.M. thesis by Kagawa [12] may be consulted for a somewhat analogous discussion based on the long cylindrical void model.

To compare the above equilibrium and crack-like solutions with the similarity solution, we make the definitions

$$s = [\sigma_\infty/(1 - d^2)]/[2\gamma_s \sin \psi/a] , \text{ and} \tag{74}$$

$$\rho = [(1 - d^2)Q(d)/d](D_s\delta_s/D_b\delta_b) . \tag{75}$$

Observe that $\sigma_\infty/(1 - d^2)$ is the average stress on the unvoided portion of the grain boundary, so that s is this stress normalized by the stress which just prevents sintering of an equilibrium-shaped void of radius a. The part of the parameter ρ that depends on $d(= a/b)$ is given in the last line of Table IV; additionally, ρ is proportional to what has been defined as Δ in (63). With these notations, the quasi-equilibrium solution (70) becomes

$$s = 1 + [h(\psi)/3 \sin \psi]\, \rho(a^3 v/B) \quad ; \tag{76a}$$

and upon linearization

$$s = 1 + (1/8)\, \rho(a^3 v/B) \quad ; \tag{76b}$$

the crack-like solution (72) is

$$s = [\sin (\psi/2)/\sin \psi][(a^3 v/B)^{1/3} + (2/3)\, \rho(a^3 v/B)^{2/3}] \quad , \tag{77a}$$

whereupon linearization gives

$$s = (1/2)(a^3 v/B)^{1/3} + (1/3)\, \rho(a^3 v/B)^{2/3} \quad . \tag{77b}$$

For the similarity solution, σ_o and σ_o' are determined by eqs. (53) and (54), and the results are inserted into (68) to solve for σ_∞. In terms of the linearized version of the stress measure s,

$$s = (1/2)[-\xi_o \eta''(\xi_o) + 1] + (1/3)\rho[-\xi_o^2 \eta'''(\xi_o) - \xi_o \eta''(\xi_o) - 1] \tag{78}$$

where it is recalled that $\xi_o^4 = 4a^3 v/B$ and, further, that a and v vary during the growth process as $t^{1/4}$ and $t^{-3/4}$ so that $a^3 v$ is constant. This feature requires that σ_∞ have a rather artificial variation with time in order to be consistent with the presumed growth history. However, our interest in the similarity solution is only in formulating a reasonable procedure for extrapolating between the quasi-equilibrium and crack-like limiting cases.

The results are shown in Fig. 7 where the similarity solution and the two limiting cases are plotted for $\rho = 1$ and $\rho = 10$. It is seen that the similarity solution approximates the equilibrium solution for low values of void growth and the crack-like solution for higher values of void growth. For both $\rho = 1$ and $\rho = 10$, the similarity solution can be thought of as a transition between the slower growing quasi-equilibrium solution and the faster growing crack-like solution for values of $(a^3 v/B)$ between 10 and 30. Note that this range of

values for (a^3v/B) is consistent with that found from a consideration of relaxation times, namely $a^3v/B \simeq 24$ at transition.

5.4 Conditions for Applicability of the Quasi-equilibrium and Crack-like Models

The solutions given in equations (76a) and (77a) are based on the assumptions that the voids grow with either a quasi-equilibrium shape or a crack-like shape, respectively. To check the consistency of these assumptions we must verify that the speeds v predicted are appropriate for the given mode of growth. Thus based on our conclusions from Fig. 7, $a^3v/B < 10$ implies growth in the quasi-equilibrium mode and $a^3v/B > 30$ implies the crack-like mode. These inequalities translate directly into inequalities on stress, since by (70) and (72) σ_∞ is a monotonic function of v.

Choosing the representative value $\psi = 75^\circ$ (Table III) equation (76a) for the quasi-equilibrium mode becomes

$$s = 1 + 0.237\rho\ (a^3v/B) \tag{79a}$$

and equation (77a) for the crack-like mode is

$$s = 0.630\ (a^3v/B)^{1/3} + 0.420\rho\ (a^3v/B)^{2/3}\ . \tag{79b}$$

Figure 8 shows a plot of eqs. (79a) and (79b) for several values of ρ. We expect that a more general solution to the problem would agree with the quasi-equilibrium solution for low values of a^3v/B making a transition between that solution and the crack-like solution near $a^3v/B = 24$. Using the value $a^3v/B = 10$ in eq. (79a), the quasi-equilibrium mode is predicted when

$$s < 1 + 2.37\ \rho\ ; \tag{80a}$$

for the crack-like mode to be effective $a^3v/B \geq 30$, hence

$$s > 1.96 + 4.06\ \rho \tag{80b}$$

implies the crack-like mode of growth.

To appreciate the restrictions involved, observe that over the range $0.1 < d < 0.5$ it is reasonable to make the approximations $(1 - d^2) \simeq 0.9$ and

$\rho \simeq 0.55\ \Delta/d$. Thus growth occurs in the equilibrium mode when

$$\sigma_\infty < 1.9(\gamma_s/a)\ (1 + 1.3\Delta/d) \tag{81a}$$

and in the crack-like mode when

$$\sigma_\infty > 3.5(\gamma_s/a)(1 + 1.2\Delta/d) \tag{81b}$$

The quantity γ_s/a is typically of the order of 1 MN/m^2 (140 psi); for example, this number follows if $\gamma_s = 1.5$ N/m and $a = 1.5$ μm. Thus for a given stress level, cavity growth in the quasi-equilibrium mode is favored when surface diffusion is much more rapid than grain boundary diffusion (i.e., when Δ is large), and also in the early stage of growth when the void radius a and the ratio d of the diameter to spacing are small. Conversely, the crack-like mode is favored when Δ is small, and in the later stages of growth when a and d are large.

Consider, for example, a stress level of 20 MN/m^2 applied across a grain boundary in a material with $\gamma_s = 1.5$ N/m, containing voids of 3 μm diameter and 12 μm center-to-center spacing; this corresponds to $d = 1/4$, i.e., approximately a 6% voidage by area of the boundary. Under these conditions the void would grow in a quasi-equilibrium mode if $\Delta > 2.0$, and a crack-like mode if $\Delta < 0.9$. Intermediate values of Δ would fit neither limiting case. When the same void has enlarged to 6 μm diameter, growth would be in the quasi-equilibrium mode if $\Delta > 7.8$ and in the crack-like mode if $\Delta < 4.3$. Finally, if we consider again the initial 3 μm void diameter, $d = 0.25$, we find that growth would occur at quasi-equilibrium conditions at all stress levels up to 100 MN/m^2 if $\Delta > 10$; on the other hand, any stress in excess of 10 MN/m^2 would cause crack-like growth if $\Delta < 0.38$.

Tables I and II have been prepared on the basis of what we think to be representative surface diffusion values, estimated for the temperatures shown

with a minimum of extrapolation from measured data. The entries in Table II show that Δ values can cover an extremely wide range and that in most cases Δ exceeds unity, sometimes substantially. Hence it will normally be the case at moderate stress levels that quasi-equilibrium or mixed conditions dominate, with crack-like conditions emerging only towards the end of growth, if at all. However, it is well to remember that D_s values for a given material and temperature can vary by several orders of magnitude [18] and that results seem to be sensitive to impurities and, of course, the environment with which the surface makes contact. Thus, we are led to believe that very low Δ values could sometimes result, and in such cases crack-like growth would occur over a wide range of stress levels and void sizes.

5.5 Rupture Time

We define a rupture time t_r as the time for a void to grow from some initial raidus a_o to the limiting radius b, at which there is coalescence. Of course, in practical cases the time required to nucleate voids is an important component of the overall rupture time (see Raj and Ashby, [8]). By using the results of previous subsections, we have approximate means of solving for the speed v of cavity growth as a function of stress σ_∞ and radius a. For example, eqs. (71) and (73), when used in conjunction with the guidelines of the last two subsections as to which case applies, provide this relation for the axisymmetric void model. The rupture time t_r is then given by

$$t_r = \int_{a_o}^{b} \frac{da}{v(a,\sigma_\infty)} \quad . \tag{82}$$

5.5.1 Growth in Crack-Like Mode

Recall that growth occurs in this mode when the inequalities (79b) or (80b) are met. The rupture time when all growth occurs in this mode is, for the axisymmetric void,

$$t_r = \frac{64}{27}\frac{b^4\Delta^3}{B}\int_{d_o}^{1}\frac{(1-u^2)^3[Q(u)]^3du}{\{[1+Q(u)\Sigma\Delta]^{1/2}-1\}^3} \tag{83}$$

where $d_o = a_o/b$ and where the stress measure Σ is defined by (65) and the function $Q(d)$ by (69). This integral cannot be carried out in closed form. However, by inspection of Table IV it is seen that Q is not strongly variable for $d > 0.1$ and it suffices to use an average value $\bar{Q} \approx 0.6$ in the integral. Indeed the integrand becomes independent of Q when $\Sigma\Delta$ is very small, and depends on the $3/2$ power of Q when $\Sigma\Delta$ is very large. Thus the replacement of Q by $\bar{Q}$ is not critical when $d_o > 0.1$ and there results

$$t_r = 0.234\,\frac{b^4}{B}\,H(d_o)\left[\frac{\Delta}{(1+0.6\Sigma\Delta)^{1/2}-1}\right]^3 , \tag{84}$$

where the function $H(d)$ is

$$H(d_o) = (35/16)\int_{d_o}^{1}(1-u^2)^3\,du = (1-d_o)[1-d_o(1+d_o)(19-16d_o+5d_o^2)/16] . \tag{85}$$

The expression for t_r has two limiting ranges. First if $0.6\Sigma\Delta < 0.5$, it is suitable to write $(1+x)^{1/2} = 1 + x/2$ and thus (84) becomes

$$t_r = 8.67(b^4/B)H(d_o)/\Sigma^3 = 3.66(b^4/B)(\gamma_s/b\sigma_\infty)^3H(d_o)\sin^3(\psi/2) \tag{86}$$

where (65) for Σ is used. Thus in this limiting case the rupture time varies as σ_∞^{-3}. Further, the result is independent of Δ, and hence of D_b, so that the rupture lifetime in this limit is controlled by the rate of surface diffusion; i.e., t_r is inversely proportional to D_s (note that B is proportional to D_s). Of course, the inequality that must be met for validity of this limit, namely $0.6\Sigma\Delta < 0.5$, implies that Δ is small. Specifically, when $\psi = 75^o$, the restriction on Δ is

$$\Delta < 0.4\,\gamma_s/b\sigma_\infty . \tag{87}$$

Hence, if we take $\gamma_s = 1.5$ N/m and $b = 6$ μm as previously, we find that

the restriction, for validity of the inverse cube relation, is $\Delta < 0.02$ when $\sigma_\infty = 5$ MN/m^2, $\Delta < 0.005$ when $\sigma_\infty = 20$ MN/m^2, $\Delta < 0.001$ when $\sigma_\infty = 100$ MN/m^2. All these combinations of σ_∞ and Δ values would, generally, be sufficient to meet the basic inequalities cited earlier for validity of the crack-like growth model. However, it is rarely, if ever, the case that such small Δ values occur (see the discussion at the end of subsection 5.4) and thus a σ_∞^{-3} law should not frequently be observed. We discuss work by Goods and Nix [19,20] on silver subsequently; in that case the data on t_r is well fit by an inverse cube law.

The other limiting case is when $0.6\Sigma\Delta > 100$. It is then appropriate to write $(1+x)^{1/2} - 1 = x^{1/2}$ and thus (84) becomes

$$t_r = 0.503(b^4/B)H(d_o)(\Delta/\Sigma)^{3/2}$$

$$= 0.327(b^4/B)(\gamma_s\Delta/b\sigma_\infty)^{3/2}H(d_o)\sin^{3/2}(\psi/2) \qquad (88)$$

Now the rupture time varies as the inverse 3/2 power of stress. Further, material parameters enter in the form $\Delta^{3/2}/B$ so that t_r is controlled by the speed of both surface and grain boundary diffusion, and is inversely proportional to $D_b^{3/2}/D_s^{1/2}$. Again setting $\psi = 75^o$, the restriction on Δ for validity of this limiting form is

$$\Delta > 76\ \gamma_s/b\sigma_\infty \quad . \qquad (89)$$

Again taking $\gamma_s = 1.5$ N/m, $b = 6$ μm, the inequality reads $\Delta > 4$ for $\sigma_\infty = 5$MN/m^2, $\Delta > 1$ for $\sigma_\infty = 20$ MN/m^2, and $\Delta > 0.2$ for $\sigma_\infty = 100$ MN/m^2. From Table II and what has been said earlier, those restrictions on Δ will typically, although not always, be met. Hence, <u>if</u> the applied stress is high enough so that the inequalities (80b) or (81b) ensuring a crack-like growth mode are met, it is to be expected that the rupture lifetime will follow a $\sigma_\infty^{-3/2}$ law. This seems consistent with results on a copper bi-crystal specimen reported by Raj [21].

For the 2-D long cylindrical void model v is given by (64), assuming that conditions for crack-like growth are met. The integral (82) for t_r can be done exactly in this case and we find

$$t_r = 0.593 \frac{b^4}{B} (1-d_o)^4 \left[\frac{\Delta}{(1+\Sigma\Delta)^{1/2}-1} \right]^3 . \tag{90}$$

This is similar to the above result for an axisymmetric void, and exhibits similar limiting stress exponents for t_r.

5.5.2 Growth in Quasi-Equilibrium and Mixed Modes

Again consider the **axisymmetric geometry.** When the inequalities (80a) or (81a) are met (i.e., for low σ_∞ or large Δ/d), growth in the quasi-equilibrium mode is insured and v is given by (71). The rupture time is calculated from (82) as

$$t_r = \frac{2kTb^3h(\psi)}{3\Omega D_b \delta_b \sigma_\infty} \int_{d_o}^{1} \frac{u(1-u^2)^2 Q(u)du}{1-2[(1-u^2)/u][\gamma_s \sin\psi/\sigma_\infty b]} . \tag{91}$$

The denominator in the integrand equals $1-1/s$, where s as defined in (74) is the ratio of the applied stress to that which just equilibrates the void against sintering. Hence, when $s >> 1$ the denominator can be replaced by unity and there results, when Q is given an average value of 0.6 as is appropriate when $d > 0.1$,

$$t_r = 0.067\ kT\ b^3 h(\psi)(1-d_o^2)^3/\Omega D_b \delta_b \sigma_\infty . \tag{92}$$

Hence the lifetime is inversely proportional to σ_∞ and to D_b. This expression must be used with care, however, because the condition $s >> 1$ will be inconsistent with the basic inequality of (80a), which must be met for validity of the quasi-equilibrium model, unless $\rho \approx 0.55\Delta/d >> 1$. When s is not large, an approximate procedure which slightly underestimates the rupture time is provided by evaluating the denominator in the integrand at its lower limit. This is equivalent to replacing

$$\sigma_\infty \text{ by } \sigma_\infty - 2(1-d_o^2)\,\gamma_s \sin\psi/bd_o$$

in the expression for t_r.

To assess the error involved when rupture time is estimated by the quasi-equilibrium model, but when the crack-like model is the more appropriate, we calculate the ratio of the rupture time prediction of (82) to that of (78), noting that the latter is appropriate for the crack-like model at representative stress levels (say, 10 to 100 MN/m^2) if Δ is of the order of unity or larger. Thus, evaluating the expressions for $\psi = 75^o$ and $d_o = 0.25$, we find

$$(t_r)_{\text{quasi-equil}}/(t_r)_{\text{crack-like}} = 0.47(\sigma_\infty b/\gamma_s\Delta)^{1/2} \quad . \tag{93}$$

Suppose that $\gamma_s = 1.5$ N/m and $b = 6$ μm as previously. Then for $\Delta = 1$ and stresses σ_∞ between 10 and 100 MN/m^2 (well beyond typical stress levels for validity of the quasi-equilibrium model), the above rupture time ratio ranges from approximately 3 to 9, and there is significant error. Of course, larger Δ values diminish the error, in proportion to $\Delta^{-1/2}$.

It may frequently happen that the early stages of void growth are best described by a quasi-equilibrium model and the later stages by a crack-like model. To estimate an a/b ratio, say d_1, at which the description of growth should change from quasi-equilibrium to crack-like, take the average of eqs. (80a) and (80b) so that

$$s = 1.5 + 3.2\rho \tag{94}$$

or approximately, for $0.1 < d_1 < 0.5$,

$$\sigma_\infty b/\gamma_s = (2.6/d_o)(1+1.2\Delta/d_1) \quad . \tag{95}$$

Choosing several representative values for Δ, Fig. 9 shows the regions in which each mode prevails. As expected, for lower values of Δ, the crack-like mode of growth prevails at lower stress levels, and conversely. To estimate rupture time assuming a process in which both modes are active, use equation (82) to obtain the time for the quasi-equilibrium portion of growth by replacing $(1-d_o^2)^3$ with $[(1-d_o^2)^3 - (1-d_1^2)^3]$, and to this add the result of equation (84) for the time spent in crack-like growth, replacing $H(d_o)$ by $H(d_1)$ in that equation.

6. Discussion of Experimental Results

Raj [21] has recently reported results of elevated temperature fracture experiments on copper bicrystal specimens containing silica and copper oxide particles along a grain boundary oriented perpendicular to the direction of tensile loading. Of the 12 specimens studied, Raj observed that 4 failed entirely or in part by the plastic-flow induced growth of holes, initiated at silica particles, and 2 failed due to "incompatibility of the matrix slip at the grain boundary." The remaining 6 specimens, for which the results are summarized in Table V, were reported to have failed by cavity growth through diffusional transport. These cavities did not initiate at the silica particles but rather at more distantly spaced copper-oxide particles, and evidence was presented to show that the voids formed very early in the deformation history.

The first two columns of Table V correspond to Raj's system for identifying the specimens; the next columns give the applied stress (labelled σ_∞ here), the temperature, one-half of the reported center-to-center spacing of the rupture cavities on the fractured grain boundary (i.e., the distance referred to as b here), and the observed time to rupture.

Comparison with theory is hindered by the lack of experimental data on D_b for Cu. The numbers listed in Table I for D_{bo} and Q_b in this case are merely estimates by Raj [21], based on analogy with other metals, but no measurement has been reported and these values may be subject to substantial errors. The surface diffusivity results, however, do result from measurements at temperatures just slightly above 750°C by Bonzel and Gjostein, reported in [18], and are consistent with results for other fcc metals, except Ag, when D_s is plotted following Gjostein against T_m/T (e.g., Fig. 17 of [18]). From these results for D_s we compute an "average" value of the dimensionless speed parameter a^3v/B by setting $a = b/2$ and evaluating v as $b/(t_r)_{obs}$,

where $(t_r)_{obs}$ is the observed rupture time in Table V. Thus

$$avg(a^3v/B) \simeq b^4/8B(t_r)_{obs} \quad .$$

Calculating B from eq. (5) and the data in Tables I and III, we show this average in the third to last column of Table V. The numbers are all large and suggest that the inequality $a^3v/B >> 24$, ensuring growth in the crack-like mode, is met for all specimens except for B7 and perhaps B1. Thus, for all but these two specimens, the rupture times should be given by eq. (84). All the quantities which enter this expression for t_r are available to us except for Δ, eq. (63), which depends on D_b. In view of the uncertainty in D_b we have adopted two approaches. First, we have attempted to fit the results for the cases of large $avg(a^3v/B)$ in Table V with a single value of Δ, taken as the same for all cases. We find that it is possible to bring the calculated rupture time, $(t_r)_{calc}$, into reasonably close agreement with the experimental results by taking $\Delta = 0.5$; this is shown by the second to last column of Table V where we list the ratios of calculated to observed times. The calculations have been based on $d_o = 0.1$. Raj does not report initial cavity (i.e., oxide particle) sizes but the calculation is not very sensitive to d_o. The value of 0.5 inferred for Δ is also consistent from the standpoint of the inequality (80b), which should be met since the observed growth seems to be in a crack-like mode. For example, taking $b = 12$ μm as representative and γ_s from Table III, we find from (81a) and (81b) that when $a = b/4$, the crack-like growth mode is ensured when $\sigma_\infty > 6.9$ MN/m^2 whereas the quasi-equilibrium mode can occur only when $\sigma_\infty < 2.8$ MN/m^2. Further, as a increases to b/2, the crack-like mode is ensured when $\sigma_\infty > 2.3$ MN/m^2 whereas the quasi-equilibrium mode can occur only when $\sigma_\infty < 1.3$ MN/m^2. Thus the adopted value of Δ is consistent with a crack-like growth mode being produced for all but the lowest stress levels in Table V (i.e., all but specimen B1 and perhaps B7).

The second approach is to adopt Raj's estimate of D_b, i.e. to use the values of D_{bo} and Q_b in Table I. Then one calculates that Δ varies with T, the results being $\Delta = 0.72$ (600°C), 1.09 (650°C), 1.58 (700°C), and 2.22 (750°C). These values for Δ have been used in calculating, from (84), the rupture times, shown in ratio to the observed times, in the last column of Table V. The agreement is less good but perhaps reasonable in view of uncertainties in material parameters. The large values of Δ are, however, consistent with a crack-like mode of growth at the stress levels of the experiments only when a is greater than about b/2. Thus it may perhaps be the case that in the temperature range of the experiments D_b values are a factor of two to three times larger than predicted on the basis of Raj's estimates; such larger D_b values (and hence smaller Δ values) seem to give a consistent explanation of the results.

Goods and Nix [19] and Goods [20] have presented creep failure results on polycrystalline silver with water vapor bubbles of 1 μm diameter spaced approximately 10 μm apart along grain boundaries. As they point out, based on a privately communicated version of our result in eq. (90) for crack-like growth of the long cylindrical void, the low stress, low Δ, limit of the crack-like model, with $t_r \propto \sigma_\infty^{-3}$, fits their data very well over the temperature range examined (200°C to 550°C). Further, as Goods and Nix [19] comment based on their own studies, the result for crack-like axisymmetric cavity growth is not very different; e.g., compare (84) and (90). By rapidly cooling a specimen immediately after fracture, so that there is no time for surface diffusion to round-out the cavities, these authors also observe that the cavities are flat and crack-like.

As Goods and Nix discuss, however, the difficulty of a direct interpretation of their results in terms of an inverse-cube expression like (86) for t_r

is that this expression is valid only when $\Delta << 1$ (see the discussion in subsection 5.4) for stress levels in the range of approximately 5 to 80 MN/m^2 as in their experiments. But the values for D_s and D_b in Table I lead to $\Delta \simeq 300$ for $T = 400^{\circ}C$, a middle-range temperature for their experiments, and a Δ value of this magnitude is inconsistent with crack-like growth. Rather than the D_{so} and Q_s values in Table I, Goods and Nix use Q_s = 20 kcal/mol (84kJ/mol) (they do not report a D_{so} value), attributing this value to a study by Gall, Gruzin, and Yudina, but they also conclude that based on D_b values for Ag, Δ is too large to justify the inverse cube relation. Goods and Nix speculate that some segregant, possibly oxygen or hydrogen, at the grain boundaries could greatly enhance the transport there, giving rise to a much lower Δ which would be consistent with the observed crack-like cavity shape.

In any event, for sufficiently small Δ (i.e., less than approximately 0.001 for the range of stresses in their experiments) the expression (84) for t_r becomes independent of Δ and reduces to (86). Using the value of Q_s noted above, Goods and Nix show that this expression predicts reasonably the dependence of t_r on σ_∞, T and b over the range examined.

7. Conclusion

We have shown how non-equilibrium aspects of surface diffusion can affect the creep cavitation process. The discussion is organized around two limiting cases: the quasi-equilibrium and the crack-like mode of cavity growth. Further, by recourse to characteristic relaxation time estimates, and to a self-similar solution for cavity growth within the linearized theory, we have shown when one model or the other applies and how to interpolate between them. More quantitative guidelines are given in Section 5 but, essentially, the quasi-equilibrium mode is favored when the stress level is low, when the cavity diameter and ratio of diameter to spacing is small, and when the parameter Δ, giving the ratio of surface to grain boundary diffusivities, is large; the crack-like mode is favored at high stresses, larger diameters, and small Δ. The parameter a^3v/B is identified as a proper dimensionless measure of speed, in order to ascertain whether the cavity is more nearly of quasi-equilibrium or crack-like shape.

The relation of applied stress to cavity growth rate is different according to the cavity shape. These relations and expressions for the rupture time are developed in Section 5. While uncertainties remain due to the lack of definitive surface and grain boundary diffusion data, the experimental results of Raj [21] on Cu bicrystals, and of Goods and Nix [19,20] on Ag polycrystals with grain boundary water vapor bubbles, exhibit features that seem consistent with our rupture time predictions based on the crack-like mode of growth.

8. Acknowledgement

The study was supported by U. S. Department of Energy (formerly Energy Research and Development Administration) under contract EY-76-S-02-3084 with Brown University. In addition, L. Sills was supported in this work by the NSF Materials Research Laboratory at Brown. We are grateful for discussions with M. F. Ashby in the early stages of the study and, more recently, with S. H. Goods, W. D. Nix, and A. G. Evans.

References

1. A. H. Cottrell, Structural Process in Creep Symposium of the Iron and Steel Institute and Institute of Metals, 8 (1961).

2. R. C. Gifkins, Proc. Tewksbury Symposium on Fracture, 44 (1965).

3. F. Garofalo, Fundamentals of Creep and Creep-Rupture in Metals, MacMillan Book Co, New York (1965).

4. D. Hull and D. E. Rimmer, Phil. Mag. 4, 673 (1959).

5. M. V. Speight and J. E. Harris, Met. Sci. J. 1, 83 (1967).

6. J. Weertman, Scripta. Met. 7, 1129 (1973).

7. F. H. Vitovec, J. Mat. Sci. 7, 615 (1972).

8. R. Raj and M. F. Ashby, Acta Met. 23, 653 (1975).

9. T.-j. Chuang, and J. R. Rice, Acta Met. 21, 1625 (1973).

10. W. W. Mullins, J. Appl. Phys. 28, 333 (1957).

11. T.-j. Chuang, Ph.D. Thesis at Brown University (1974).

12. K. I. Kagawa, Sc.M. Thesis at Brown University (1976).

13. P. G. Shewmon, Diffusion in Solids, McGraw Hill, New York (1963).

14. W. W. Mullins, J. Appl. Phys. 30, 77 (1959).

15. V. Vitec, Acta Met., to be published.

16. C. Herring, J. Appl. Phys. 21, 437 (1950).

17. C. Herring, The Physics of Powder Metallurgy, ed. W. E. Kingston, McGraw Hill, 143 (1951).

18. G. Neumann and G. M. Neumann, Surface Self-Diffusion of Metals, Diffusion Information Center, (1972).

19. S. H. Goods and W. D. Nix, Acta Met. 26, 739 (1978).

20. S. H. Goods, Ph.D. Thesis at Stanford University (1977).

21. R. Raj, Acta Met. 26, 341 (1978).

22. C. J. Smithells and E. A. Brands, Metals Reference Book, Butterworth, London (1976).

23. H. W. King, Physical Metallurgy, North-Holland (1970).

24. J. P. Hirth and J. Lothe, Theory of Dislocations, McGraw-Hill, New York, 764 (1968).

25. E. H. Kennard, Kinetic Theory of Gases, McGraw-Hill, New York (1938).

26. J. Weertman, Acta Met. 5, 1743 (1974).

27. C. Herring, Structure and Properties of Solid Surfaces, ed. R. Gomer and and C. S. Smith, Univ. Chicago Press (1952).

28. Y. C. Fung, Foundations of Solid Mechanics, Prentice-Hall, New Jersey, 195 (1965).

Appendix: Characteristic Relaxation Times for Matter Transport

In order to determine the conditions for which self-diffusion along the surface of the void and along the grain boundary ahead of the void are the only significant mechanisms of matter transport, it is useful to compare the characteristic relaxation time for each mode of transport which results from a periodic disturbance. Mullins [10,14] derived characteristic times for the flattening of a periodic, two-dimensional free surface; the extension to three dimensions (Section A1), as well as an examination of the characteristic relaxation time for grain boundary self-diffusion (Section A2) are presented here. In addition, the rigid grain assumption is examined in Section A3.

A1. Mass Transport at a Surface

Indeed, there are several mechanisms which may contribute to the process of mass transport at a surface: namely, surface self-diffusion, lattice self-diffusion, and evaporation-condensation. To calculate characteristic relaxation times for these processes, consider a semi-infinite, isotropic solid occupying the half-space $z \geq w$, where w is a surface given by

$$w(x,y,t) = A(t) \exp [2\pi i(x/\ell + y/L)] \qquad (A1)$$

with ℓ and L being the wavelengths of the periodic disturbance in the x and y directions respectively, and $A(t)$ taken to be much smaller than both ℓ and L.

Conservation of mass at the surface requires that

$$\partial(J_s)_x/\partial x + \partial(J_s)_y/\partial y + J_z + \Delta\theta = (1/\Omega)(\partial w/\partial t) \qquad (A2)$$

where $(J_s)_x$ and $(J_s)_y$ are surface fluxes, J_z is the lattice flux in the

z direction and $\Delta\theta = \theta - \theta_o$ where θ_o is the rate of evaporation from a flat surface. In linear diffusion theory the fluxes in equation (A2) are given by

$$(J_s)_{x,y} = -(D_s\delta_s/\Omega kT)\ \partial\mu/\partial x,\partial y \quad , \quad J_z = -(D_\ell/\Omega kT)\ \partial\mu/\partial z \qquad (A3)$$

where D_ℓ is the coefficient of lattice diffusion.

For a free surface, the chemical potential is given by Eq.(2). Since the slope of the surface is everywhere small,

$$(\mu)_{surface} = \mu_o - \Omega\gamma_s c^2 w(x,y,t) \qquad (A4)$$

where $c^2 = (2\pi/\ell)^2 + (2\pi/L)^2$. Following Mullins [14] and Herring [27] if we assume that the flow within the crystal is essentially divergenceless (short relaxation time for attainment of local vacancy equilibrium), then μ must satisfy Laplace's equation, and

$$\mu = \mu_o - \Omega\gamma_s c^2 \exp(-cz)w(x,y,t). \qquad (A5)$$

To complete the analysis of equation (A2), we again follow Mullins [14] and consider the matter transport which results from the process of evaporation-condensation. From kinetic theory [25], the flux from the surface can be approximated by

$$\Delta\theta = \Delta p/(2\pi mkT)^{1/2} \qquad (A6)$$

where $\Delta p = p - p_o$, p being the vapor pressure at the surface, p_o the pressure at a reference state, and m is the mass of a molecule. Presuming the surface to be in equilibrium with its own vapor at this pressure p, that the vapor is a perfect gas, and that p is close to p_o

$$\mu \simeq \mu_o + kT(\Delta p/p_o). \qquad (A7)$$

Equating the chemical potential of the solid phase (A4) to that of the vapor phase (A7) at the surface, with both referred to the same reference state, implies that

$$\Delta p/p_o = -(\Omega\gamma_s c^2/kT)\ w(x,y,t)\ .$$

Therefore, equation (A5) becomes

$$\Delta\theta = -[p_o\Omega\gamma_s c^2/(2\pi m)^{1/2}(kT)^{3/2}]\ w(x,y,t) \qquad (A8)$$

Substitution of equations (A3), (A5) and (A8) into equation (A2) leads to a differential equation for the amplitude of the disturbance as

$$A'(t) + (F_s c^4 + F_\ell c^3 + F_v c^2)\ A(t) = 0 \qquad (A9)$$

where

$$F_s = D_s\delta_s\Omega\gamma_s/kT$$

$$F_\ell = D_\ell\Omega\gamma_s/kT$$

and

$$F_v = p_o\Omega^2\gamma_s/[(2\pi m)^{1/2}(kT)^{3/2}]\ .$$

Solution of equation (A9) gives the shape of the free surface as

$$w(x,y,t) = a_o\exp[-(F_s c^4 + F_\ell c^3 + F_v c^2)t]\ \exp[2\pi i(x/\ell + y/L)]; \qquad (A10)$$

indeed, each of the terms in the first exponential of equation (A10) gives the contributions to the flattening of the periodic surface by surface self-

diffusion, lattice self-diffusion and evaporation-condensation, respectively. From equation (A10) it is seen that the characteristic relaxation time for each mode of transport is given by

$$\tau_s = (kT/D_s\delta_s\Omega\gamma_s)(1/c^4) \tag{A11}$$

for surface self-diffusion,

$$\tau_\ell = (kT/D_\ell\Omega\gamma_s)(1/c^3) \tag{A12}$$

for lattice self-diffusion, and

$$\tau_v = [(2\pi m)^{1/2}(kT)^{3/2}/p_o\Omega^2\gamma_s](1/c^2) \tag{A13}$$

for evaporation-condensation.

An estimate of the contribution to the total atom flux on a free surface for each of these mechanisms can be made by examining the ratios of the characteristic relaxation times. Equations (A11) and (A12) imply that

$$\tau_s/\tau_\ell = (D_\ell/D_s\delta_s)(1/c) \ . \tag{A14}$$

Assuming the wavelengths of the disturbance to be the same in the x and y directions (i.e. $\ell = L = \lambda$), equation (A14) reduces to

$$\tau_s/\tau_\ell = (D_\ell/D_s\delta_s)(\lambda/2\sqrt{2}\,\pi). \tag{A15}$$

Similarly, equations (A11) and (A13) imply that

$$\tau_s/\tau_v = \{p_o\Omega/[D_s\delta_s(2\pi mkT)^{1/2}]\}(1/c^2) \tag{A16}$$

or for $\ell = L = \lambda$

$$\tau_s/\tau_v = \{p_o\Omega/[2D_s\delta_s(2\pi mkT)^{1/2}]\}(\lambda/2\pi)^2 \qquad (A17)$$

If $\tau_s/\tau_\ell << 1$ and $\tau_s/\tau_v << 1$ for a given λ, surface diffusion can be expected to be the dominant mechanism of matter transport for free surface disturbances of wavelength less than λ. For some common metals, Table II lists values of λ_{max} for these ratios of relaxation times equal to 0.1. These maximum wavelengths are all within reasonable bounds for the consideration of intergranular voids. Hence it can be concluded that surface self-diffusion is the only mechanism which need be considered for the temperatures of interest in this study.

A2. Matter Transport in the Grain Boundary

A similar analysis will be pursued in order to study the dominant mode of mass transport at the grain boundary. Consider a local grain boundary thickening δ and its associated normal stress distribution σ_n on the grain interface produced by placing matter selectively along the grain boundary. Generalizing Weertman's [26] 2-dimensional analysis, the grain interface can be modelled as the surface of a semi-infinite, isotropic, linear elastic solid occupying the half-space $z \geq 0$. If the stresses at the surface are of the form

$$\sigma_n = \sigma_{zz} = B(t)\exp[2\pi i(x/\ell + y/L)] \qquad (A18)$$

and

$$\sigma_{yz} = \sigma_{xz} = 0 \ ,$$

the linear elastic solution (Fung [28]) gives a grain boundary thickening

$$\delta = -2(1-\nu)\sigma_n/Gc \qquad \text{(A19)}$$

where $c^2 = (2\pi/\ell)^2 + (2\pi/L)^2$, and $[(1-\nu)/G]B(t)$ is assumed much smaller than 1; G is the elastic shear modulus and ν the Poisson ratio.

Mass transport at the grain boundary can result from either grain boundary or lattice diffusion; hence conservation of mass at the grain boundary requires that

$$\partial(J_b)_x/\partial x + \partial(J_b)_y/\partial y + 2(J_z) = -(1/\Omega)(\partial\delta/\partial t) \qquad \text{(A20)}$$

where $(J_b)_x$ and $(J_b)_y$ are the grain boundary fluxes in the x and y directions respectively, J_z is the lattice flux in the z direction and $\partial\delta/\partial t$ is the grain boundary thickening rate. As before, the fluxes can be related to the chemical potential through the following relations

$$(J_b)_{x,y} = -(D_b\delta_b/\Omega kT)\ \partial\mu/\partial x,\partial y, \qquad J_z = -(D_\ell/\Omega kT)\partial\mu/\partial z\ . \qquad \text{(A21)}$$

By an argument similar to that in Section A1, the chemical potential throughout the entire crystal is found to be

$$\mu = \mu_o - \Omega\sigma_n \exp(-cz)\ . \qquad \text{(A22)}$$

Substitution of equations (A21), (A22), (A18) and (A19) into equation (A20), leads to a first order linear ordinary differential equation for $B(t)$. Solution of this equation reveals the characteristic relaxation time for grain boundary diffusion to be

$$\tau_b = [2(1-\nu)/G]\ (kT/D_b\delta_b\Omega)(1/c^3) \qquad \text{(A23)}$$

and the characteristic relaxation time for lattice self-diffusion to be

$$\tau_\ell = [(1-\nu)/G](kT/D_\ell\Omega)(1/c^2) \ . \qquad (A24)$$

Comparing these relaxation times shows that

$$\tau_b/\tau_\ell = 2(D_\ell/D_b\delta_b)(1/c) \qquad (A25)$$

or for $\ell = L = \lambda$

$$\tau_b/\tau_\ell = (D_\ell/D_b\delta_b)(\lambda/\sqrt{2}\,\pi) \ . \qquad (A26)$$

If $\tau_b/\tau_\ell << 1$ for a given λ, grain boundary diffusion will be the dominant mechanism of matter transport near grain boundary disturbances of wavelength less than λ. Table II gives λ_{max} for some common metals with $\tau_b/\tau_\ell = .1$; it is seen that for these metals grain boundary diffusion is expected to be the dominant mechanism of matter transport.

A3. Elastic Effect

Appropriateness of the rigid grain assumption will be examined by comparing the (elastic) relaxation time of the grain boundary with a time which is computed on the basis of the rigid grain assumption. From the analysis in Section 5 which is based on a rigid grain model, equation (61) says that

$$v \simeq (D_b\delta_b\Omega/kT)[1/a(b-a)]\sigma_{net}$$

where v is the void growth rate for the two-dimensional equilibrium configuration, and σ_{net} is the net section stress. A representative time τ_r based on this model can be defined as

$$\tau_r \equiv (b-a)/v = (1/\sigma_{net})(kT/D_b\delta_b\Omega)[a(b-a)^2] \ . \qquad (A27)$$

From equation (A23) for the (elastic) grain boundary relaxation time

$$\tau_b/\tau_r \approx [(b-a)/a](\sigma_{net}/G) \ . \qquad \text{(A28)}$$

Since the net section stress is much smaller than the shear modulus, $\tau_b << \tau_r$; thus effects resulting from elastic deformation become neglibibly small after a time which is short in comparison with that for which the process of void growth is active.

Table I [(i)]. Material Properties of Some Common Metals

Metals		Ag	Cu	αFe	γFe	Ni	Zn
T_m(°K)	[22]	1234	1356	1809	1809	1726	694
$\Omega(m^3) \times 10^{29}$	[23]	1.706	1.181	1.177	1.177	1.094	1.524
m(kg) $\times 10^{25}$	[22]	1.79	1.06	0.93	0.93	0.97	1.09
E(Pa) $\times 10^{-10}$	[22]	7.58	12.40	19.60	19.6	20.70	9.70
ν	[22]	0.38	0.35	0.28	0.28	0.31	0.43
(ii) $D_{so}(m^2/sec)$	[18]	4.5×10^{-6}	3.4×10^{-2}	10.0	0.4	2.85×10^{-2}	9.4×10^{-6}
Q_s(kcal/mol)		11.7	38.2	55.6	49.0	37.7 ± 3.8	6.7
Temperature Interval (°K)		470° - 770°	1070° - 1180°	1020° - 1370°	1170° - 1370°	885° - 1110°	340° - 460°
(iii) $D_{bo}(m^2/sec)$	[22]	1.2×10^{-5}	10^{-5} (vii)	2.5×10^{-4}	3.4×10^{-4}	1.75×10^{-6}	2.2×10^{-5}
Q_b(kcal/mol)		21.5	24.8 (vii)	40.0	39.0	28.2 ± 2	14.3
Temperature Interval (°K)		623° - 753°	-	803° - 923°	1191° - 1287°	1123° - 1373°	348° - 433°
$D_{\ell o}(m^2/sec)$	[22]	6.7×10^{-5}	7.8×10^{-5}	2.0×10^{-4}	4.9×10^{-5}	1.27×10^{-4}	1.3×10^{-5}
Q_ℓ(kcal/mol)		45.2 ± 0.2	50.4 ± .2	60.0	67.86 ± 1.45	67.2	21.9
Temperature Interval (°K)		913° - 1228°	971° - 1334°	973° - 1023°	1443° - 1634°	1143°-1677°	513° - 691°

Table II [(i)] Calculated Values of Δ and λ_{max} at $T = .5T_m$ and $T = .8T_m$

Metals	Ag	Cu	αFe	γFe	Ni	Zn
At $T = .5T_m$						
$\Delta = D_s\delta_s/D_b\delta_b$	5.72×10^{2}	7.9×10^{-2}	3.09	2.05 (iv)	28.4 (iv)	1.30×10^{4}
p_o(Pa) [22]	5.3×10^{-6}	3.8×10^{-6}	10^{-7}	10^{-7}	7.4×10^{-7}	2.6×10^{-6}
λ_{max}(μm) (for $\tau_s/\tau_\ell = .1$)	1.13×10^{7} (iv)	8.1×10^{2} (iv)	1.17×10^{2}	5.96×10^{4} (iv)	1.31×10^{6} (iv)	5.98×10^{5} (iv)
λ_{max}(μm) (for $\tau_s/\tau_v = .1$)	8.4×10^{2}	7.4	2.18×10^{2}	2.74×10^{2} (iv)	3.86×10^{2}	1.26×10^{3}
λ_{max} (μm) (for $\tau_b/\tau_\ell = .1$)	9.89×10^{3} (iv)	4.5×10^{4}	1.89×10^{1}	1.45×10^{4} (iv)	2.31×10^{4} (iv)	2.30×10^{1} (iv)
At $T = .8T_m$						
$\Delta = D_s\delta_s/D_b\delta_b$	$1.41 \times 10^{-1\pm1}$ (iv),(vi)	3.2	8.02×10^{1} (iv)	1.6×10^{1}	8.64 (v)	2.08×10^{2} (iv)
p_o (Pa) [22]	2.9×10^{-2}	6.2×10^{-2}	2.3×10^{-4}	2.3×10^{-4}	8.5×10^{-3}	4.1
λ_{max}(μm) (for $\tau_s/\tau_\ell = .1$)	$1.98 \times 10^{\pm1}$ (vi)	2.6×10^{1}	4.67×10^{1} (iv)	1.16×10^{3}	7.89×10^{1} (v)	1.53×10^{2} (iv)
λ_{max} (μm) (for $\tau_s/\tau_v = .1$)	5.38 (vi)	1.3×10^{1}	1.69×10^{3}	1.07×10^{3}	4.9×10^{1} (v)	7.0 (iv)
λ_{max} (μm) (for $\tau_b/\tau_\ell = .1$)	7.03 (iv)	3.8×10^{1}	2.91×10^{-1} (iv)	3.52×10^{1}	4.56	3.69×10^{-1} (iv)

Footnotes for Tables I and II

(i) Diffusion parameters were generally chosen so that the temperature ranges for the various types of diffusion processes would be (a) made to overlap and (b) near as possible to $0.5T_m$ and/or $0.8T_m$. Note that in finding the diffusion coefficient (D_s, D_b or D_ℓ) extrapolation far outside the given temperature may lead to erroneous results.

(ii) Note that values for surface diffusion parameters are rather suspect with wide ranges in both the pre-exponential term D_{so} and the activation energy Q_s.

(iii) D_{bo} calculated assuming $\delta_b = 5 \times 10^{-10}$ m.

(iv) Calculated on the basis of Table I; values for diffusion parameters, however, are outside the desired temperature range by more than 10%.

(v) Calculated for $D_{so} = 4.16 \times 10^{-2}$, $Q_s = 47.7$, $1373 < T < 1523$.

(vi) Calculated for $D_{so} = 10^{2\pm1}$, $Q_s = 55.3$, $970 < T < 1220$.

(vii) Estimated in [21]; measurement not available.

Table III. Values of γ_b, γ_s and ψ for Some Common Metals, from [24]

Material	$\gamma_b(\frac{\text{joules}}{m^2})$	$\gamma_s(\frac{\text{joules}}{m^2})$	$\psi = \cos^{-1}\frac{\gamma_b}{2\gamma_s}$
Ag	0.79	1.14	1.22
Au	0.36	1.485	1.45
Cu	0.65	1.725	1.38
Fe	0.78	1.950	1.37
Ni	0.69	1.725	1.37

Table IV

Values of the function Q(d) appearing in solution for axisymmetric void growth; d = a/b = ratio of cavity diameter to average center-to-center spacing.

d	0	0.01	0.05	0.10	0.20	0.40	0.60	0.80	1.00
Q	0	0.12	0.34	0.48	0.61	0.65	0.61	0.55	0.50
$(1-d^2)Q/d$	∞	11.6	6.78	4.76	2.93	1.36	0.65	0.25	0

Table V. Comparison of Data by Raj [21], on Diffusive-Mode Fractures of Cu Bicrystals, with Predictions of Crack-like Model.

Batch	Spec No.	σ_∞ (MN/m^2)	T($^\circ$C)	b(μm)	$(t_r)_{obs}$ (s)	avg($a^3 v/D$)*	$(t_r)^{\dagger}_{calc}/(t_r)_{obs}$	$(t_r)^{\dagger\dagger}_{calc}/(t_r)_{obs}$
I	B1	1	700	16	1.60×10^6	146	5.9	20
I	B2	13	700	10	4.63×10^4	770	0.6	2.9
II	B7	5	750	8.5	1.18×10^5	64	0.4	2.4
III	B8	10	700	12	7.03×10^4	1052	1.0	4.5
III	B9	10	650	13	1.98×10^5	1411	1.2	3.2
III	B10	10	600	13.5	4.31×10^5	2336	1.8	2.9

* Average value corresponds to $a = b/2$; computed from surface diffusion data of Table I and observed rupture time, using $b^4/8Bt_r$.

† Calculated from eq. (84) for the crack like model using $d_o = 0.1$ and surface diffusion data of Table 1, and assuming $\Delta = 0.5$ in all cases.

†† Calculated from eq. (84) as for previous column, but obtaining Δ from the estimate (no measurement available) for D_b by Raj [21]; $\Delta = 0.72$ (600°C) , 1.09 (650°C), 1.58 (700°C), 2.22 (750°C).

Figures

Fig. 1 (a) Quasi-equilibrium void and (b) crack-like void, each situated along the grain boundary; $\pi-\psi$ denotes the angle between the tangent to the void at the void tip and the x-axis.

Fig. 2 Grain boundary thickening δ which occurs if grains behave (a) rigidly or (b) elastically.

Fig. 3 Axisymmetric void shapes predicted by the similarity solution for $\xi_o = 1, 2, 3$ and the quasi-equilibrium solution.

Fig. 4 Axisymmetric void shape predicted by the crack-like and similarity solutions for (a) $\xi_o = 8$ and (b) $\xi_o = 16$.

Fig. 5 Graph of (a) non-dimensionalized curvature (κ_1) at the void tip and (b) non-dimensionalized flux at the void tip, each vs. the non-dimensionalized void growth rate a^3v/B for the axisymmetric void as computed from the quasi-equilibrium, similarity and crack-like solutions.

Fig. 6 (a) Cross-section of 2-D periodic array of voids along the grain boundary. (b) View of grain boundary containing axisymmetric voids with an average center-to-center spacing $2b$.

Fig. 7 Graph of non-dimensionalized stress vs. void growth rate at $\rho = 1$ and 10 for the linearized quasi-equilibrium, self-similar, and crack-like solutions.

Fig. 8 Graph of non-dimensionalized stress vs. void growth rate at several values of ρ for the quasi-equilibrium and crack-like solutions with $\psi = 75^o$.

Fig. 9 Graph of non-dimensionalized stress vs. non-dimensionalized void radius at which void growth becomes crack-like. Arrows indicate the direction in which each mode of growth is applicable; similarly directed arrows can be attached to each curve.

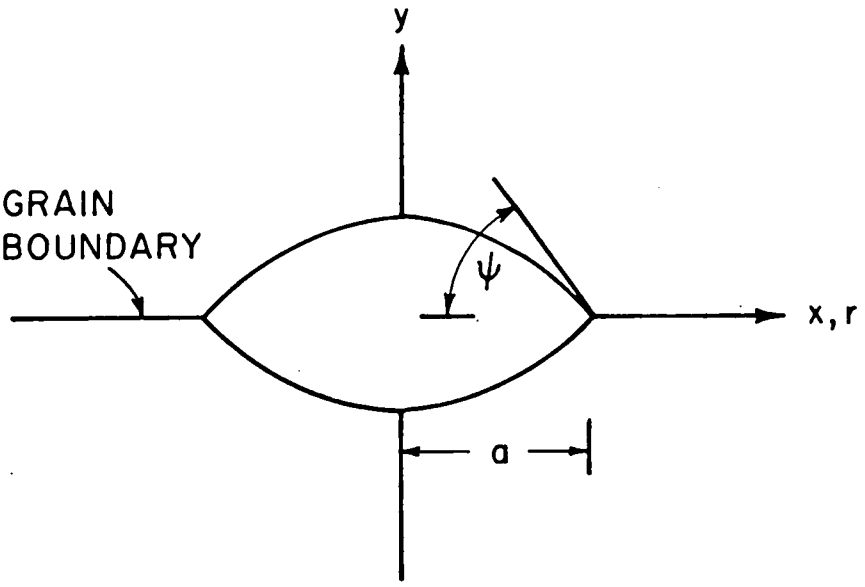

(a)

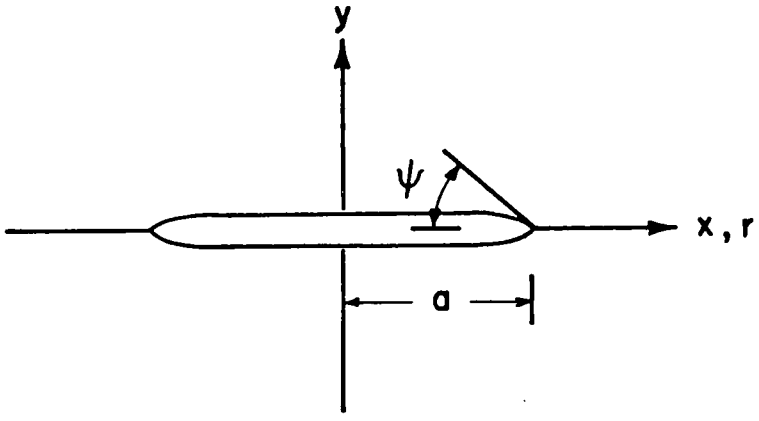

(b)

Figure 1

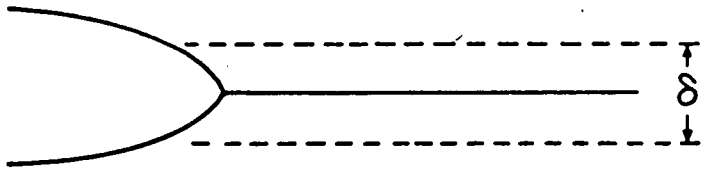

(a)

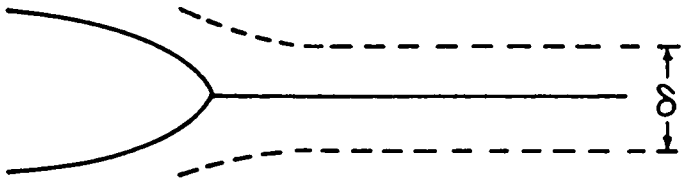

(b)

Figure 2

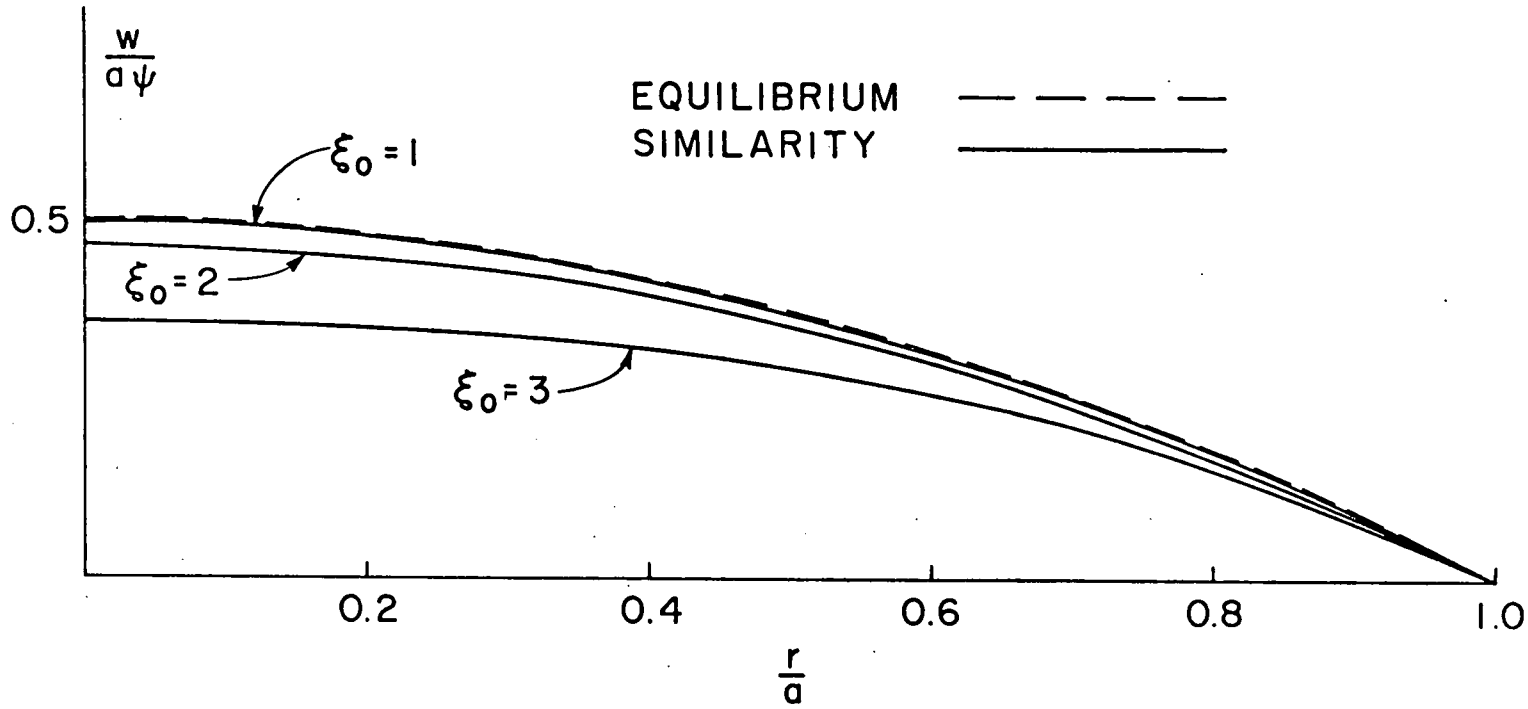

Figure 3

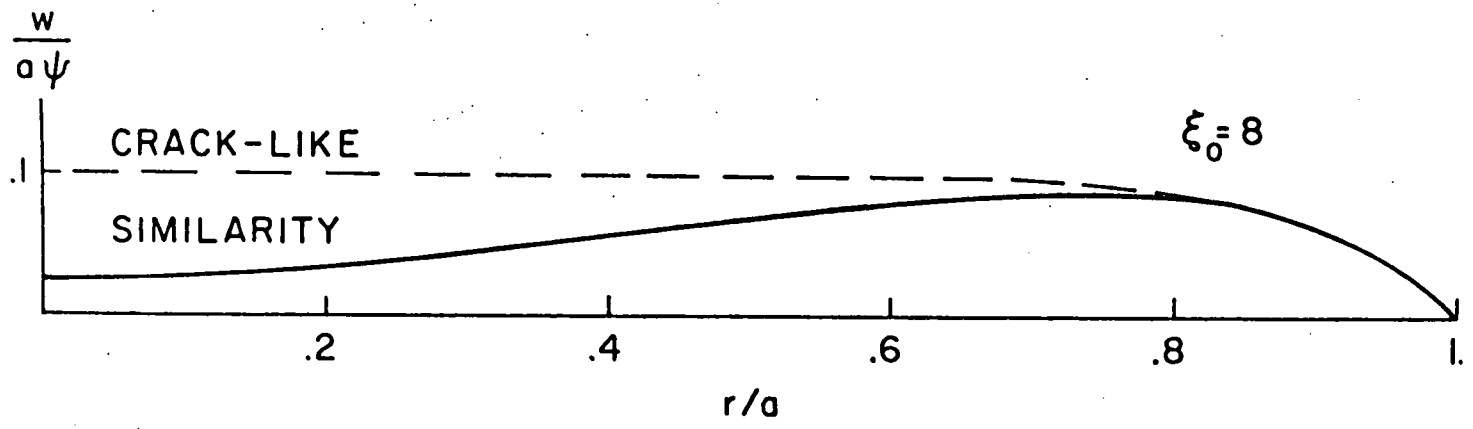
w/aψ
CRACK-LIKE
SIMILARITY
ξ0 = 8
.1
.2
.4
.6
.8
1.
r/a

(a)

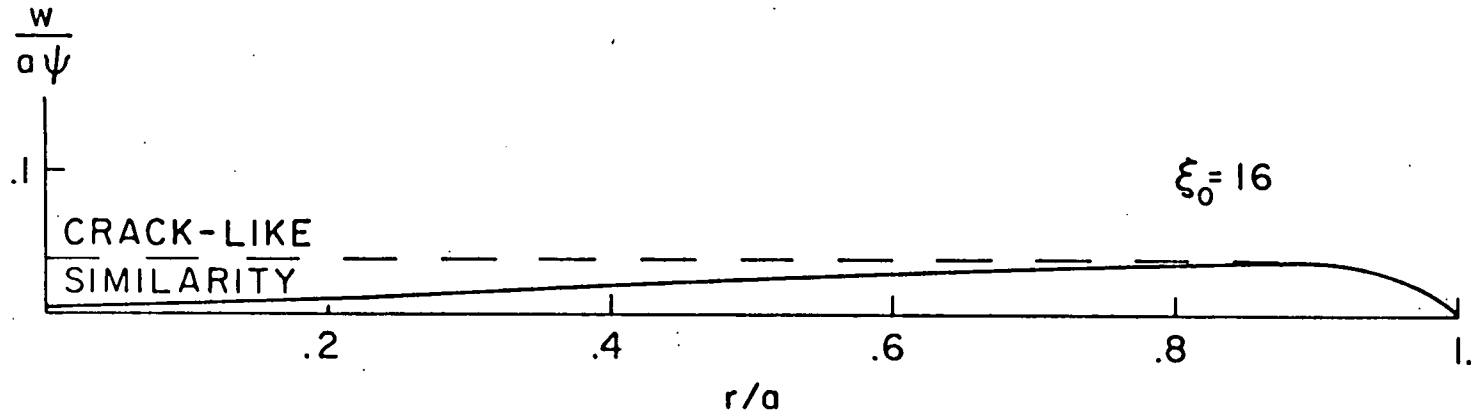
w/aψ
.1
CRACK-LIKE
SIMILARITY
ξ0 = 16
.2
.4
.6
.8
1.
r/a

(b)

Figure 4

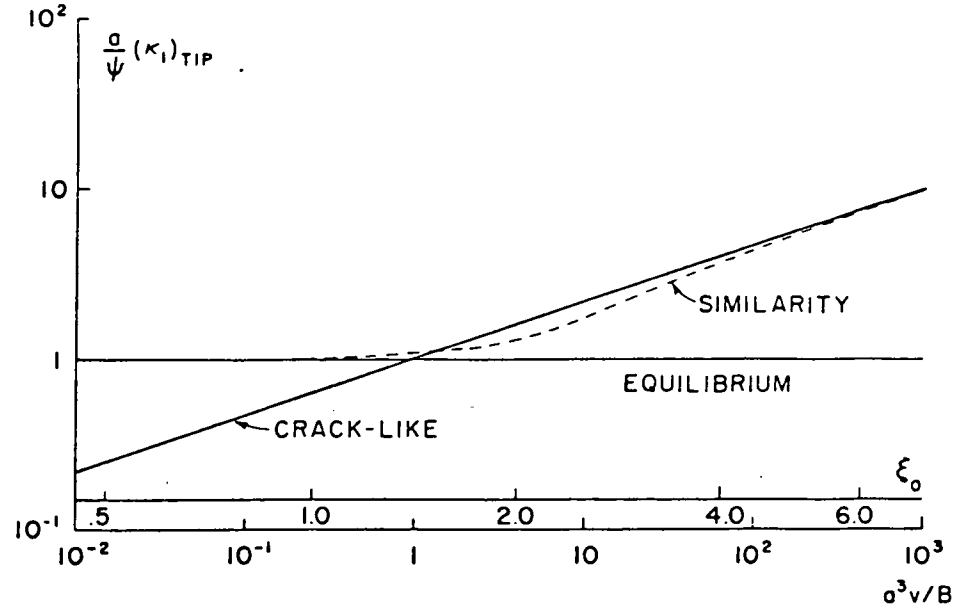
10^2
$\frac{a}{\psi}(\kappa_1)_{TIP}$
10
1
10^{-1}
SIMILARITY
EQUILIBRIUM
CRACK-LIKE
ξ_o
.5
1.0
2.0
4.0
6.0
10^{-2}
10^{-1}
1
10
10^2
10^3
a^3v/B

(a)

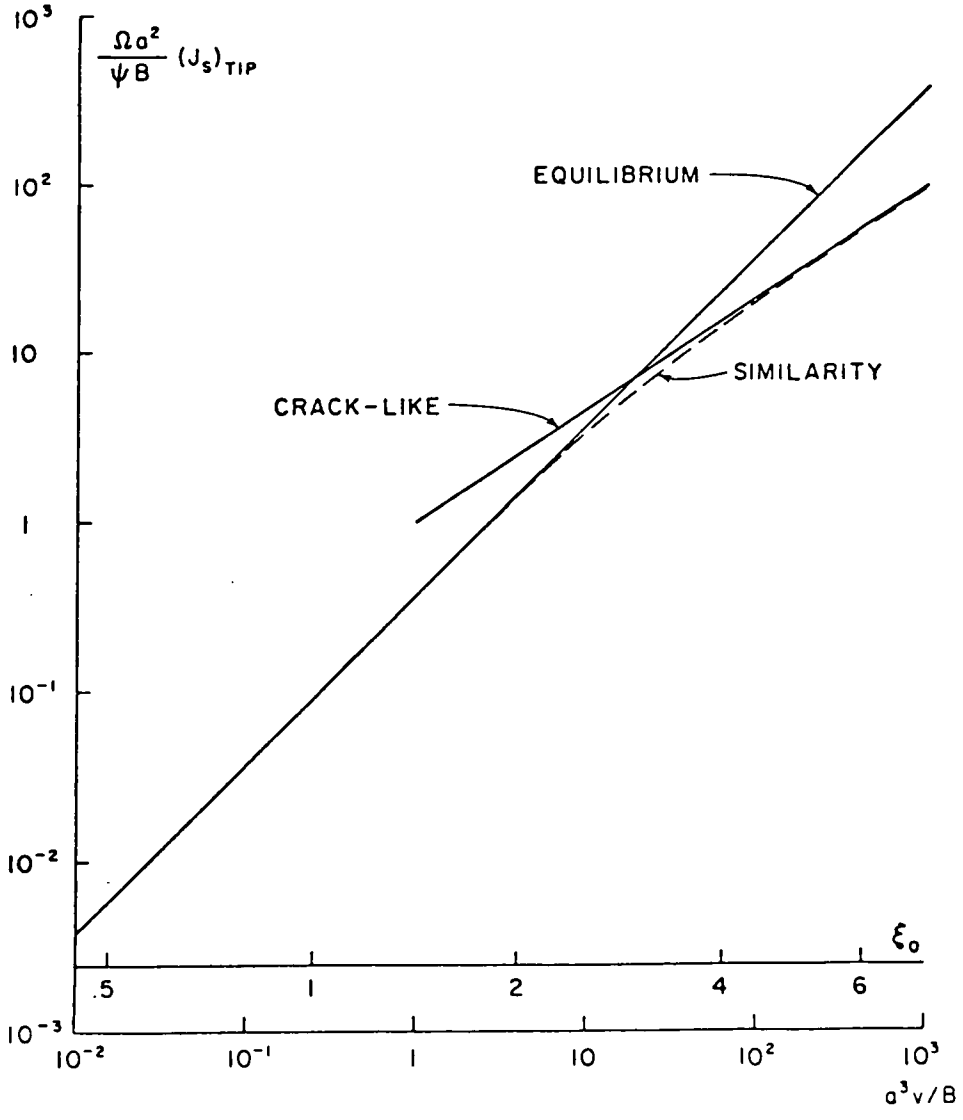
10^3
$\frac{\Omega a^2}{\psi B}(J_s)_{TIP}$
10^2
10
1
10^{-1}
10^{-2}
10^{-3}
EQUILIBRIUM
SIMILARITY
CRACK-LIKE
ξ_o
.5
1
2
4
6
10^{-2}
10^{-1}
1
10
10^2
10^3
a^3v/B

(b)

Figure 5

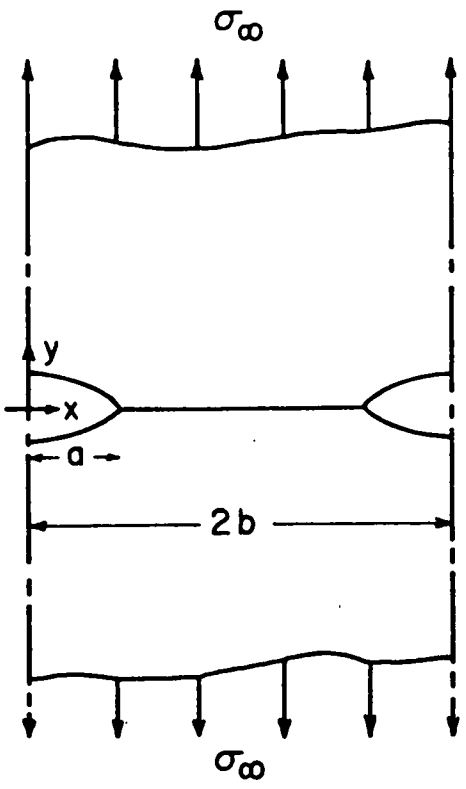

(a)

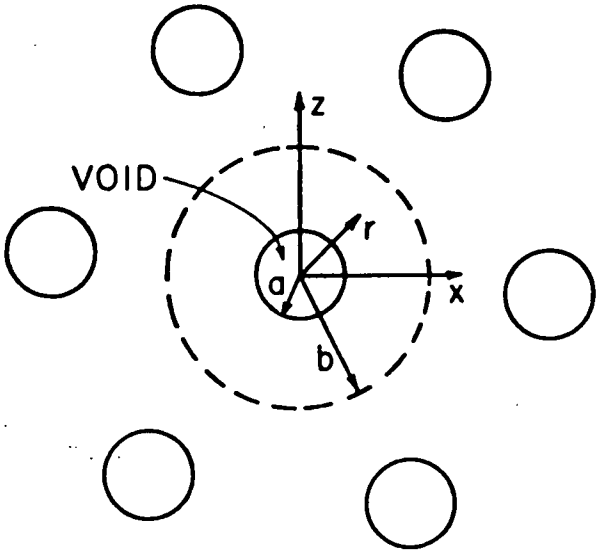

(b)

Figure 6

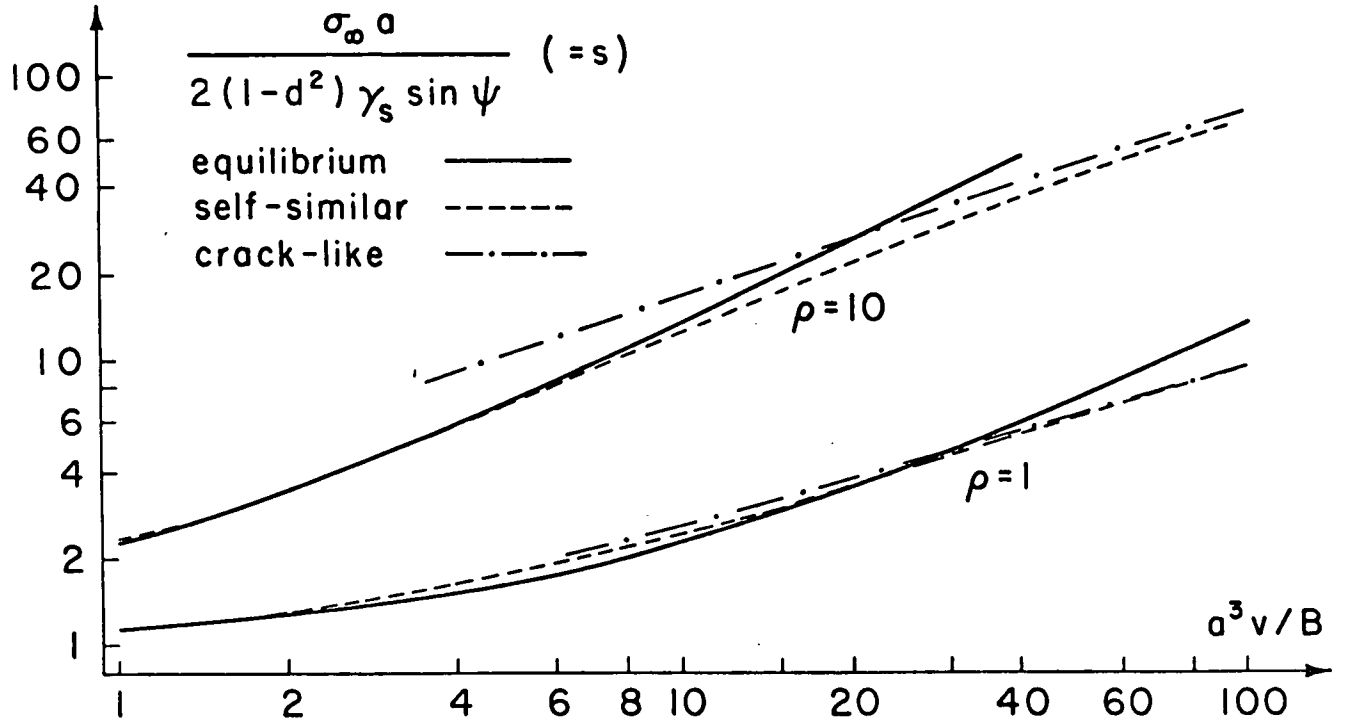
$\frac{\sigma_\infty a}{2(1-d^2)\gamma_s \sin\psi}$ (=s)
equilibrium
self-similar
crack-like
ρ=10
ρ=1
$a^3 v/B$
100
60
40
20
10
6
4
2
1
1
2
4
6
8
10
20
40
60
100

Figure 7

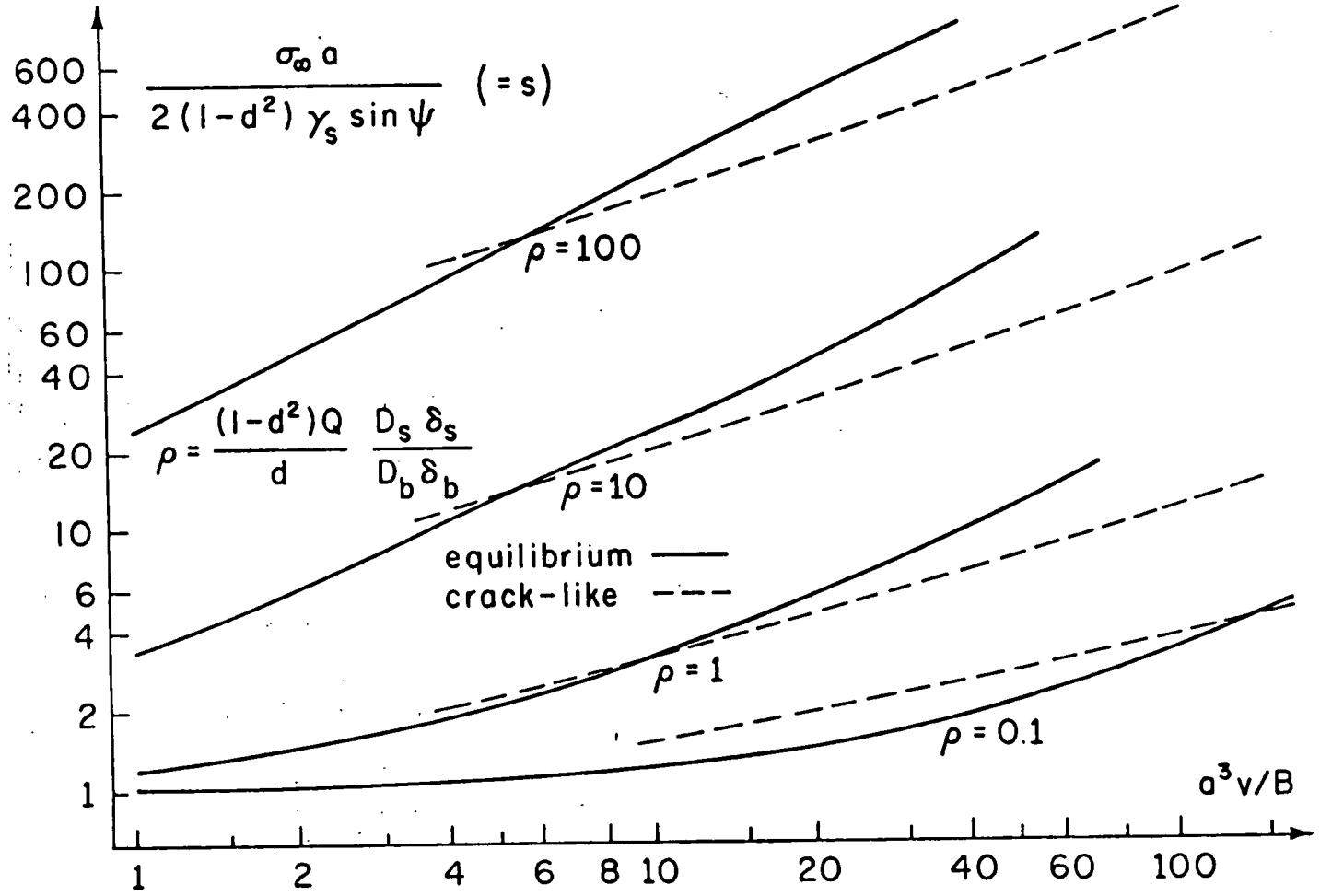
600
400
200
100
60
40
20
10
6
4
2
1
$\frac{\sigma_\infty a}{2(1-d^2)\gamma_s \sin\psi}$ (=s)
$\rho = \frac{(1-d^2)Q}{d} \frac{D_s \delta_s}{D_b \delta_b}$
ρ=100
ρ=10
ρ=1
ρ=0.1
equilibrium
crack-like
$a^3 v/B$
1
2
4
6
8
10
20
40
60
100

Figure 8

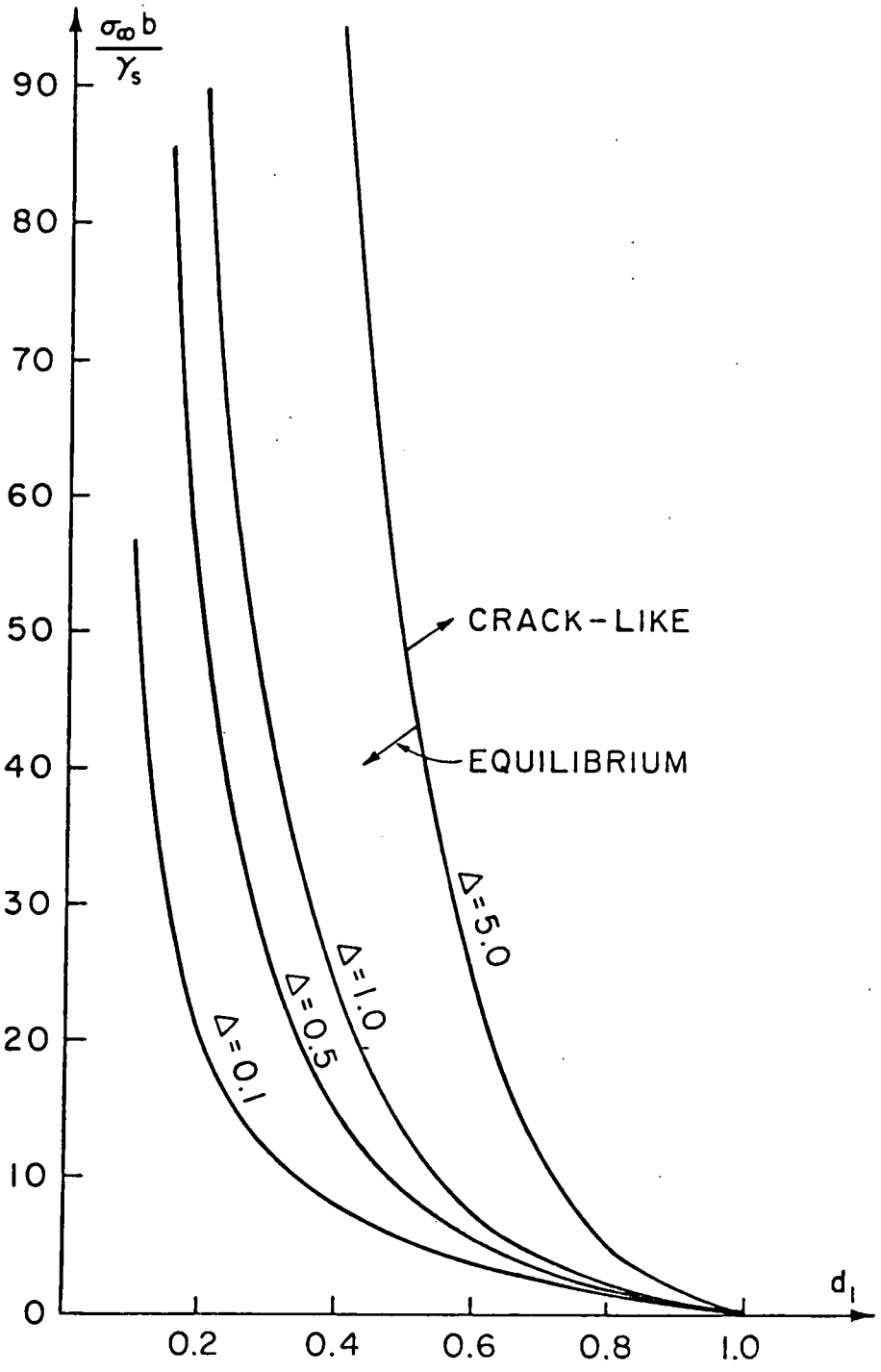
$\frac{\sigma_\infty b}{\gamma_s}$
90
80
70
60
50
40
30
20
10
0
0.2
0.4
0.6
0.8
1.0
d_1
CRACK-LIKE
EQUILIBRIUM
Δ=5.0
Δ=1.0
Δ=0.5
Δ=0.1

Figure 9